scientific reports

Check for updates

OPEN

Energy transfer and multicolour photoluminescence in phosphors La_2O_3 doped by Tm^{3+}, Ho^{3+}, and Eu^{3+} for white LED and security applications

Praful P. Khode[1], Aditi Deshmukh[1], Mateusz Czerwiński[2], Marta Michalska-Domańska[2]✉ & S. J. Dhoble[1]✉

As the world evolves, the demand for efficient lighting sources is rising rapidly, and to cater to the burgeoning demand for swift expansion, technological advancement in white light-emitting diodes (WLEDs) and lighting materials is crucial. In this work, the photoluminescence of La_2O_3 single-doped (Tm, Ho, Eu), double-doped and triple-doped phosphors prepared by combustion synthesis was studied. XRD confirms hexagonal phase (-P6c2c) with lattice contraction on doping, supported by Rietveld refinement, while SEM shows agglomerated particles (~ 12 µm) and FTIR confirms La–O bonding. Under UV excitation, Tm^{3+}, Ho^{3+} , and Eu^{3+} give blue, green, and orange-red emission, respectively; in Ho^{3+} doped samples, the small $^5F_4$–$^5S_2$ gap (~ 200 cm^{-1}) compared to host phonon energy (~ 400 cm^{-1}) leads to merged emission. Efficient energy transfer (Tm → Ho, Ho → Eu, Tm → Eu) is observed in co-doped and tri-doped systems, with La_2O_3:Tm/Ho/Eu phosphor showing a strong red component. These results suggest La_2O_3—based phosphors are promising candidates for WLEDs, barcode security, and multicolour LED applications.

Keywords White light-emitting diodes (WLEDs), Barcode Security, Energy transfer, Photoluminescence, Lanthanum oxide phosphors, Rare-earth doping, Lattice contraction

In the era of rapid paradigm shifts, the demand for efficient lighting sources is increasing exponentially. To accommodate the demographic imperative of growing population, technological advancements in white light-emitting diode (WLEDs) and lighting technologies are needed. LED applications demand different parameters: CCT tuning provides warm (low CCT) or cold (high CCT) white light for ambience and efficiency; color purity ensures vivid, accurate display and lighting performance; and balancing these enables LEDs to meet needs ranging from cozy indoor lighting to bright outdoor and high-precision display applications[1,2]. Luminescent phosphors have widespread applications in lighting devices such as fingerprint detection[3], barcode security [4], biomedical applications[5], anti-counterfeiting[6], radiation dosimetry[7], solar energy conversion[8], displays[7], scintillators[9], Leaser [10]and phototherapy[11]. Red deficiency in WLEDs phosphor in commercial phosphor can one of the problem in modern lighting devices [12,13].

Rare earth elements are considered modern industrial vitamins because they are applicable in the development of new technologies. Rare earth elements are used in fields of catalysis, chemical industry, metallurgy, LED technology and green energy. Rare earth elements have a vacant 4f. shell that contributes to their excellent optical, electrical, ceramic, magnetic ,thermal and chemical properties[14,15]. Among all rare earth elements, La_2O_3 is financial efficient and easily available rare earth element. La_2O_3 is p-type semiconductor with a band gap of 4.3 eV, and it has strongest basicity. La_2O_3 possesses a relatively low phonon energy of about 400 cm^{-1}, which facilitates the merging of two closely spaced energy levels with a gap smaller than 400 cm^{-1}[16–18]. This results in a single emission peak with a larger full width at half maximum (FWHM), thereby reducing non-radiative losses in the host lattice. This makes it a highly exemplary prospect for rare-earth doping in the preparation of efficient phosphor materials. La_2O_3 in the hexagonal phase has a single site to replace the dopant in host lattice which

[1]Department of Physics, R.T.M. Nagpur University, Nagpur 440033, India. [2]Institute of Optoelectronics, Military University of Technology, Kaliskiego Street, 00-908 Warszawa, Poland. ✉email: marta.michalskadomanska@gmail.com; sjdhoble@gmail.com

make it more prominent candidate for sharp emission bands[19–22]. Refractive index is an essential parameter for studying the optical properties of the prepared sample. It provides valuable insight into how light is absorbed, scattered, and confined within photoactive materials. In the present work, La_2O_3(Lanthanum oxide) acts as the host matrix, and its high refractive index contributes to enhanced light–matter interaction, improved optical transparency, and efficient energy transfer within the doped system [23].

The emission spectra of prepared phosphor depend on the host lattice and the dopant. The choice of dopant depends on the application or the objective of synthesis. Dopants like europium (Eu) emit blue and red light in + 2 and + 3 oxidation states, respectively [24,25]. Lanthanide dopants give sharp emission peaks , while transition metals like Bi and Mn^{2+} give blue emission [26]. The incorporation of dopant ions into the host lattice also depends strongly on the ionic radii of both the dopant and host atoms. A closer match in their ionic radii facilitates effective substitution and minimizes lattice distortion, thereby improving the structural stability and optical performance of the La_2O_3-based material [27].The emission of phosphor also depends on the lattice (host). C.X. Chen et al. studied the Bi/Tb/Sm doped $CaY_2Al_4SiO_{12}$ phosphor prepared by the high-temperature solid state reaction method. The prepared phosphor was used for WLEDs applications with high colour rendering index 87 and a low correlated color temperature (CCT, 4747.56 K) [28]. Govind B. Nair et al. prepared up conversion Ceramic phosphors $Tm_{2-x}WO_6$:$_xYb^{3+}$ using solid state method. They studied the emission of Tm doped phosphor at excitation wavelength 980 nm [29].

Combustion synthesis method is rapid , safe, energy efficient, taking less time [12,30],suitable for large-scale production, and cost effective method as compare to other method. Gases releases during the synthesis helps make prepare material porous. Porous nature help to enhance the optical property [31,32].

In this study , we synthesized the La_2O_3 doped with Tm, Ho, and Eu phosphor by combustion synthesis using hydrazine as fuel. We carried out structural characterization using XRD(x-ray diffraction), morphological study using SEM (scanning electron microscopy), EDX (Energy-Dispersive X-ray) for elemental study, optical study using (photoluminescence), and bond vibration is studied using FT-IR (Fourier-Transform Infrared spectroscopy). This study mainly focuses on development on green, red, blue and WLEDs phosphors.

Synthesis

We synthesized lanthanum dioxide (La_2O_3) using a combustion method, with adding various rare earth dopants. The synthesis process involved both individual and co-doping strategies, culminating in triple-doping trials to evaluate the influence of multiple dopants on the material properties. Initially, lanthanum nitrate [$La(NO_3)_2$] was dissolved in distilled water and stirred using a magnetic stirrer to obtain a homogeneous precursor solution at 300 rpm. In parallel, the selected dopants (Tm, Eu, and Ho) are each dissolved in nitric acid within separate test tubes and subjected to mild heating in a hot air oven to ensure complete dissolution. Once the dopants were fully dissolved, they were gradually introduced into the lanthanum nitrate solution under constant stirring to achieve uniform mixing. Following this, hydrazine hydrate (5 mL) was added as a fuel to initiate the combustion reaction. The resulting solution was transferred to a china dish and placed in a preheated vertical furnace at 550 °C. This intermediate product was then manually ground using a mortar and pestle to ensure fine and consistent particle size. The ground material was subsequently calcined in a muffle furnace at 800 °C. The synthesized La_2O_3 samples—undoped, singly doped, co-doped, and triply doped—were then subjected to further characterization and testing to evaluate their structural, morphological, and optical properties. The schematic representation of the synthesis is shown in Fig. 1.

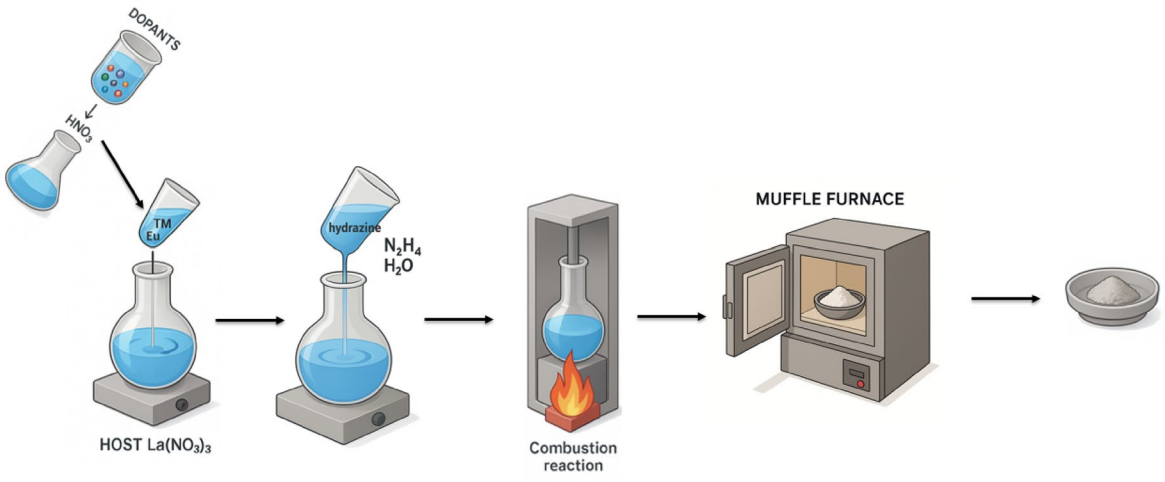

Fig. 1. Schematic representation of combustion synthesis.

Results and Discussion:

XRD analysis

The XRD pattern of the prepared sample was recorded using an instrument Rigaku Miniflex D 600. XRD machine is enabled with Cu Kα radiation (λ = 0.154056 nm), operating at 40 kV and 15 mA. The XRD patterns were recorded from 10 ^{0} to 80 ^{0} at 0.04 ^{0} step size. Figure 2 shows the XRD pattern of La_2O_3, La_2O_3:Tm/Ho, La_2O_3:Tm/Ho,La_2O_3:HO/Eu, and La_2O_3:Tm/Ho/Eu . The concentration of dopant La_2O_3: Tm^{3+}(1.5 mol%)/ Ho^{3+}(0.5 mol%), La_2O_3: Ho^{3+}(1.5 mol%)/Eu^{3+}(2.0 mol%), La_2O_3:Tm^{3+}(1.5 mol%)/Eu^{3+}(1.0 mol%), and La_2O_3: Tm^{3+}(1.5 mol%)/Ho^{3+}(1.0 mol%)/Eu^{3+}(4.0 mol%) were selected so that they have maximim energy transfer eiffecncy at that concentration. All XRD spectra of prepared phosphor were well matched with the standard ICDD data file no 01–074-2430. Impurity such as Eu_2O_3 , Ho_2O_3, and Tm_2O_3 used in the synthesis does

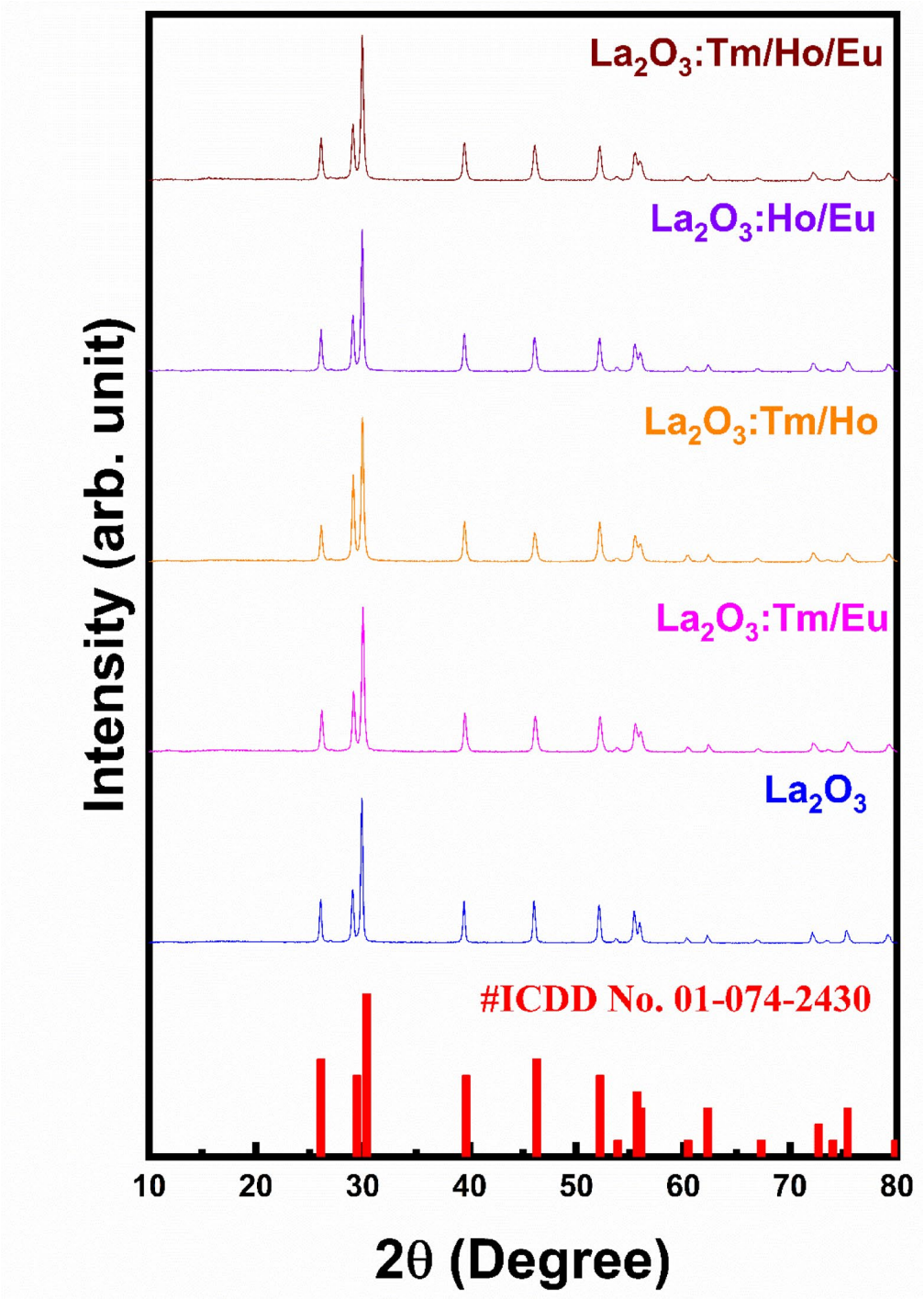

Fig. 2. XRD pattern of La_2O_3, La_2O_3:Tm/Ho, La_2O_3:Tm/Ho, La_2O_3:Ho/Eu, and La_2O_3:Tm/Ho/Eu with the standard data.

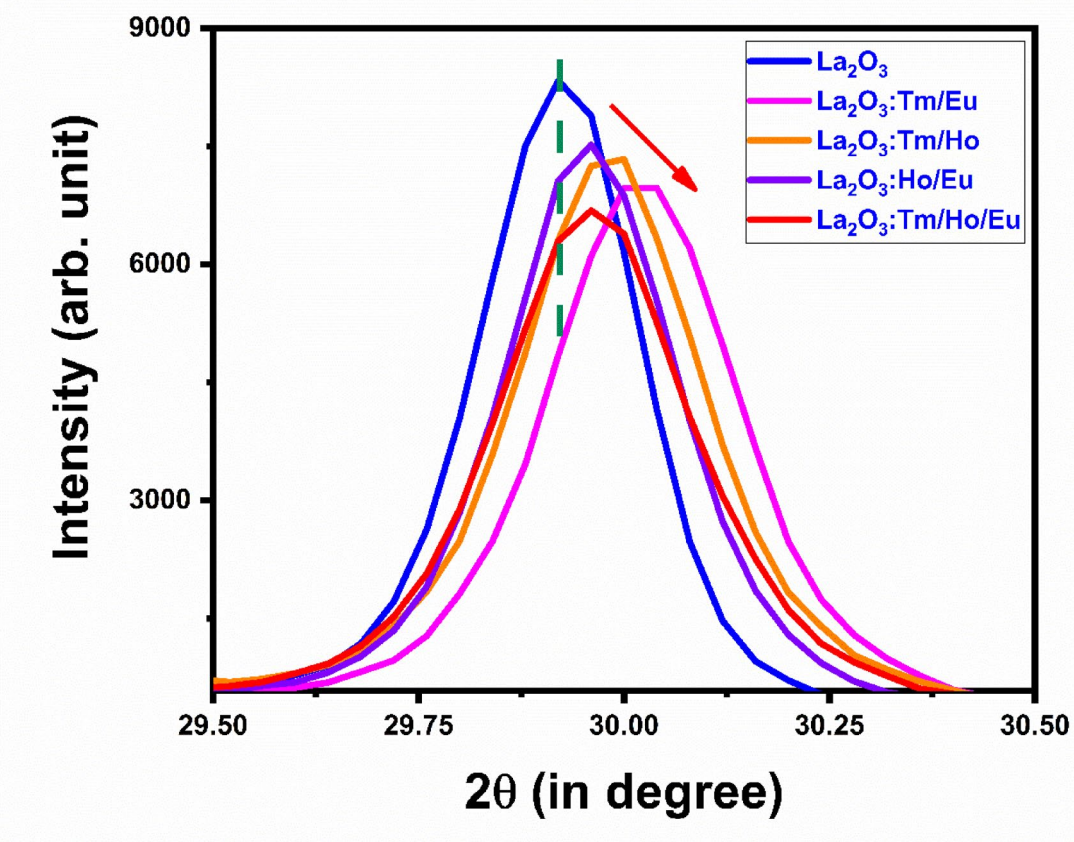

Fig. 3. XRD shift in pattern of La_2O_3, La_2O_3:Tm/Ho, La_2O_3:Tm/Ho, La_2O_3:Ho/Eu, and La_2O_3:Tm/Ho/Eu.

Crystalline Size				
La_2O_3	La_2O_3:Tm/Ho	La_2O_3:Tm/Eu	La_2O_3:Ho/Eu	La_2O_3:Tm/Ho/Eu
80.47968115 nm	61.41207426 nm	58.25336 nm	67.455 nm	55.33576 nm

Table 1. Crystalline Size of La_2O_3, La_2O_3:Tm/Ho, La_2O_3:Tm/Ho,La_2O_3:Ho/Eu, and La_2O_3:Tm/Ho/Eu.

not induce any impurity peak or add other phase. This confirms that the added impurities were completely incorporated into the host lattice. The XRD peaks of all prepared samples are sharp, demonstrating the high crystalline nature of the prepared phosphors. The prepared phosphors crystallized in a hexagonal structure with the space group -P 6c 2c. The addition of dopants into the host lattice did not change the phase and space group of the co-doped phosphor.

Figure 3 shows the shifting of the XRD pattern of La_2O_3,La_2O_3:Tm/Ho, La_2O_3:Tm/Ho, La_2O_3:HO/Eu, and La_2O_3:Tm/Ho/Eu . The shifting of the XRD patterns toward higher angles is due to the addition of impurities like Eu (0.947 Å), Ho (0.901 Å), and Tm (0.880 Å) which have smaller ionic radii compared to La (1.032 Å). The shift occurs due to the lattice contraction in host lattice due to the addition of the impurities in the host lattice having the ionic radii smaller than that of the host [33,34]. Order of ionic radii of ions are La > Eu > Ho > Tm. In the shifting graph, La_2O_3:Tm/Eu and La_2O_3:Tm/Ho has maximum shift from La_2O_3 due to the larger mismatch in ionic radii. The introduction of dopants into the lattice tends to reduce the crystallinity of prepared samples. The FWHM of the doped samples is larger than that of pure La_2O_3, which indicates an increase in lattice strain or defects in the crystal structure. The crystalline size of pure La_2O_3 is larger than that of the co-doped phosphor. La_2O_3:Ho/Eu has the maximum crystalline size while La_2O_3:Tm/Ho/Eu has the minimum crystalline size in co-doped phosphor. The detailed crystalline size is shown in table: Crystalline Size of La_2O_3 has maximum size of 80.47968115 nm and minimum at La_2O_3:Tm/Ho/Eu with 55.33576 nm. Adding dopant, in crystal structure leads to decreases in crystalline Size from 80.47968115 nm to 55.33576 nm as shown in Table 1.

The effect of doping on the crystal structure of the prepared sample was studied by using Rietveld refinement. The Rietveld refinement of La_2O_3, La_2O_3:Ho/Eu, La_2O_3:Tm/Ho, La_2O_3:Tm/Ho, and La_2O_3:Tm/Ho/Eu are shown in Fig. 4a–e respectively. The Rietveld refinement was carried out using full proof software by assuming a peak shape Pseudo-Voigt profile function and linear background. The parameters of rietveld refinement such as Rp, $R_{wp,}$ R_{exp} , and χ^2 are mentioned in Table 2. Doping led to changes in lattice parameters, and the refined

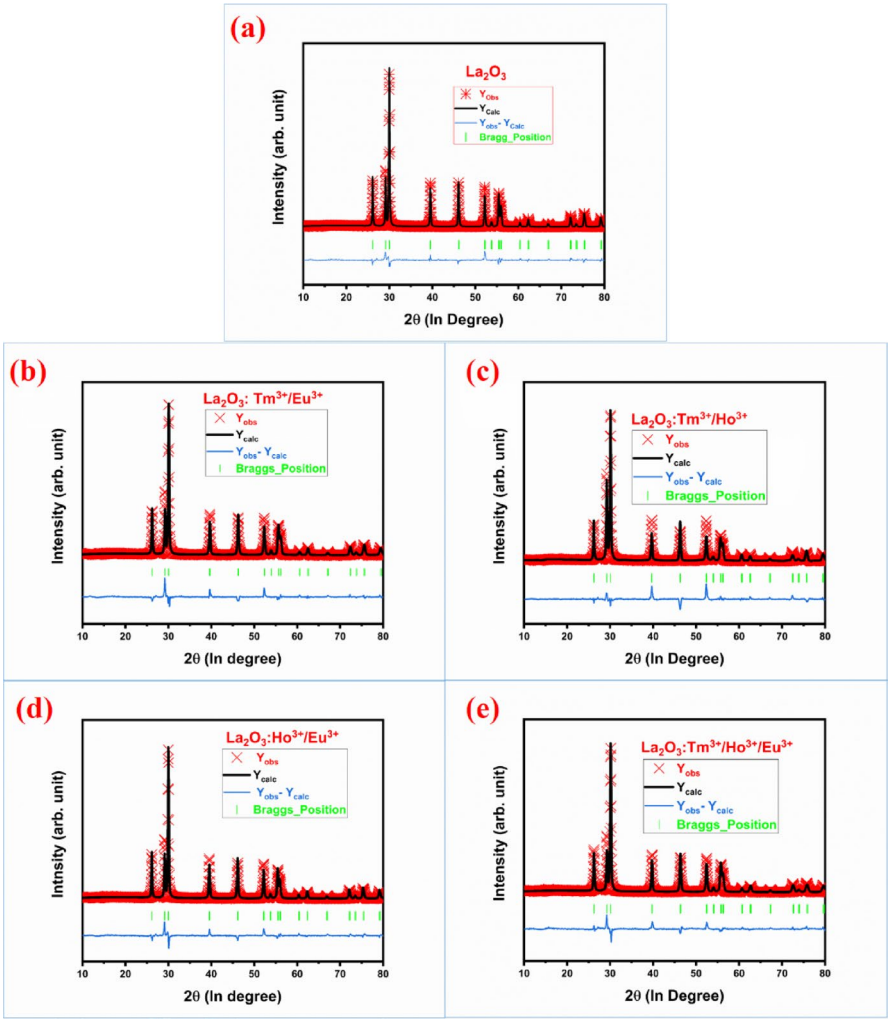

Fig. 4. Rietveld refinement of La_2O_3, La_2O_3:Tm/Ho, La_2O_3:Tm/Ho La_2O_3:Ho/Eu, and La_2O_3:Tm/Ho/Eu.

Sr no	Name	R_p	R_{wp}	R_{exp}	χ^2
1	La_2O_3	17.5	16.6	9.93	2.79
2	La_2O_3:Tm/Ho	20.1	20.7	9.72	4.54
3	La_2O_3:Ho/Eu	18.8	17.5	10.17	2.94
4	La_2O_3:Tm/Eu	18.4	17.4	10.14	2.93
5	La_2O_3:Tm/Ho/eu	19.0	17.7	10.31	2.94

Table 2. Rp, R_{wp}, R_{exp} , and χ^2 parameter of reitveld refinement.

parameters compared with the standard data are shown in Table 3. The effect of doping on the position of atom in crystal structure is shown in Table 4. The addition of dopants is in such small quantities that does not reflect in crystal structure. The crystal structure La_2O_3, La_2O_3:Ho/Eu, La_2O_3:Tm/Ho, La_2O_3:Tm/Ho, and La_2O_3:Tm/Ho/Eu is shown in Fig. 5a–e, respectively.

The addition of dopants does not alter the hexagonal phase of the crystal structure. All the prepared samples show no alteration in α and γ because nearly the same radii ion that is replaced as a dopant. The variation in parameters a and c shows a reducing trend compared to the pure phosphor. This reduction occurs because smaller-radius dopants shrink the lattice structure. La_2O_3:Tm/Ho/Eu shows the maximum variation in lattice parameter due to maximum shrinking in crystal structure compared to other prepared phosphors. Position of atoms in crystal after Rietveld refinement is shown in Table 4. In the hexagonal phase of La_2O_3, there is only one crystallographic site for La^{3+} ions in the lattice. Therefore, dopants like Tm^{3+}, Ho^{3+}, and Eu^{3+} has only one cryptographically identical site present in the lattice. The position of atoms also indicates that the ions like Tm^{3+}, Ho^{3+}, and Eu^{3+} replace the position of La^{3+} in the lattice. Oxygen is placed in two different cryptographically identical positions and is present in the crystal i.e. O1 and O2. The site of O1 does not change by adding dopant,

Sr no	Name	La_2O_3	La_2O_3:Tm/Ho	La_2O_3:Ho/Eu	La_2O_3:Tm/Eu	La_2O_3:Tm/Ho/eu	Standard
1	a (Å)	3.937225	3.922530	3.935604	3.925273	3.916989	3.9373
2	c (Å)	6.130284	6.110597	6.131602	6.115010	6.103198	6.1299
3	α (In degree)	90.000 °	90.000 °	90.000 °	90.000 °	90.000 °	90.000 °
4	γ (In degree)	120 °	120 °	120 °	120 °	120 °	120 °
5	Volume ($Å^3$)	82.2985	81.4229	82.2484	81.5958	82.2964	82.30

Table 3. Lattice parameter of La_2O_3, La_2O_3:Tm/Ho, La_2O_3:Tm/Ho ,La_2O_3:Ho/Eu, and La_2O_3:Tm/Ho/Eu with standard data.

Sr no	Name	Element	X	Y	Z
1	La_2O_3	La1	0.33330	0.66670	0.24521
		O1	0.00000	0.00000	0.00000
		O2	0.33330	0.66670	0.66609
2	La_2O_3:Tm/Ho	La1	0.33330	0.66670	0.23400
		O1	0.00000	0.00000	0.00000
		O2	0.33330	0.66670	0.70283
		Tm1	0.33330	0.66670	0.23400
		Ho1	0.33330	0.66670	0.23400
3	La_2O_3:Tm/Eu	La1	0.33330	0.66670	0.24016
		O1	0.00000	0.00000	0.00000
		O2	0.33330	0.66670	0.65989
		Tm1	0.33330	0.66670	0.24016
		Eu1	0.33330	0.66670	0.24016
4	La_2O_3:Ho/Eu	La1	0.33330	0.66670	0.24557
		O1	0.00000	0.00000	0.00000
		O2	0.33330	0.66670	0.66297
		Ho1	0.33330	0.66670	0.24557
		Eu1	0.33330	0.66670	0.24557
5	La_2O_3:Tm/Ho/Eu	La1	0.33330	0.66670	0.24971
		O1	0.00000	0.00000	0.00000
		O2	0.33330	0.66670	0.66439
		Tm1	0.33330	0.66670	0.24971
		Ho1	0.33330	0.66670	0.24971
		Eu1	0.33330	0.66670	0.24971

Table 4. Atom position of La_2O_3, La_2O_3:Tm/Ho, La_2O_3:Tm/Eu, La_2O_3:Ho/Eu, and La_2O_3:Tm/Ho/Eu.

while the z coordinate of O2 changes as we add dopant. In the first type of O^{2-} coordination site, each oxygen ion is bonded to four chemically equivalent La^{3+} ions, forming OLa_4 tetrahedra. These tetrahedra are connected by sharing corners with six OLa_6 octahedra, sharing corners with another six OLa_4 tetrahedra, and sharing edges with three OLa_6 octahedra as well as three OLa_4 tetrahedra. In the second O^{2-} site, the oxygen is coordinated to six La^{3+} ions, resulting in OLa_6 octahedra. These octahedra connect through edge-sharing with six similar OLa_6 octahedra, sharing corners with twelve OLa_4 tetrahedra, and also sharing edges with six OLa_4 tetrahedra. Figure 4a shows the crystal structure of La_2O_3.

SEM and EDX analysis

Figures 6a–c show the SEM images of La_2O_3 at 10, 10, and 2 micrometer magnification, respectively. The particle seems to be agglomerate due to uncontrolled heating during the calcination process. The particles are porous in nature, due to the release of gases during calcination and combustion. The gases released during synthesis are O_2 , NH_3, and water vapor. The particles exhibit irregular shapes and sizes. Figure 6d shows the particle size distribution of the prepared La_2O_3. The average particle size of prepared phosphor is 12 micrometer. Larger particle size is due to agglomeration of particles. The porous nature of the particles is useful in lighting applications. Figure 6e shows the EDX spectra of La_2O_3. EDX spectra conation peaks due to the La (lanthanum) and O (Oxygen) that confirm the formation of La_2O_3.

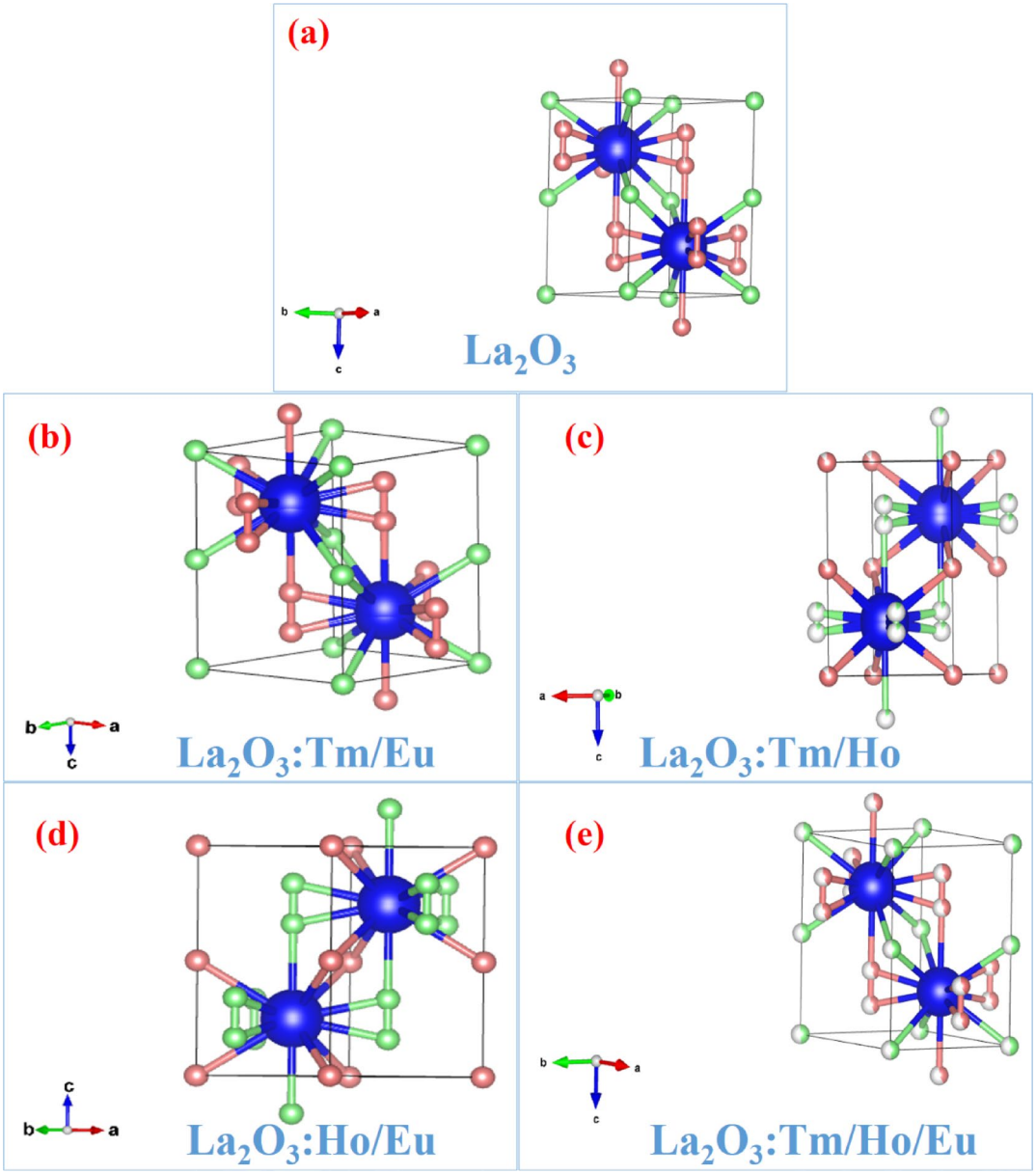

Fig. 5. Crystal structure of La_2O_3, La_2O_3:Tm/Ho, La_2O_3:Tm/Ho , La_2O_3:Ho/Eu, and La_2O_3:Tm/Ho/Eu.

PL analysis

La_2O_3:Eu

Figure 7 shows the excitation spectra of La_2O_3: Eu^{3+} at different concentration of Eu ion varying from 1 mol% to 5 mol %. The excitation spectra were recorded from 220 to 480 nm at emission wavelength fixed at 627 nm. The excitation spectra contain one major peak at 291 nm and several minor peaks at 363 nm, 383 nm, 395 nm, and 467 nm. The broad peak from 220 to 333 nm is centered at 291 nm is due to the charge transfer phenomenon between Eu^{3+} to O^{2-}. This excitation range is in mercury execution so it is hazardous for environment and it is not useful foe LEDs (Light Emitting Diode) application. Peak at 363 nm, 383 nm, 395 nm, and 467 nm is due to $^7F_0 \rightarrow 5D_4$, $^7F_0 \rightarrow 5G_6/5L_6$, $^7F_0 \rightarrow 5L_6$, and $^7F_0 \rightarrow 5D_2$ transitions. Transition respectively. Selection of peak at 395 nm is due to. maximum intensity and fall under UV-range (300 -400 nm) is very useful for led application[25].

The emission spectra of La_2O_3: Eu^{3+} is recorded at the excitation wavelength 395 nm from 525 to 650 nm as shown in Fig. 8. The emission spectra are recorded for different concentration of Eu^{3+} such as 1.0 mol %,2.0 mol%, 3.0 mol%, 4 mol%, and 5.0 mol%. The emission spectra contain one major peak at 627 nm and several minor peaks at 539 nm, 580 nm, 587 nm, 596 nm, and 614 nm. Peak at 580 nm is due to $5D_0 \rightarrow 7F_0$ transition. Peak at 587 nm, 596 nm is due to $5D_0 \rightarrow 7F_1$ transition and peak at 614 nm and 627 nm is due to $5D_0 \rightarrow 7F_2$ transition[25,35]. Two peaks at a single transition are due to stark splitting. Intensity of emission spectrum increases from 1 mol% to 4 mol%. At 4 mol% it shows maximum intensity, then after that the intensity of spectrum decreases as shown

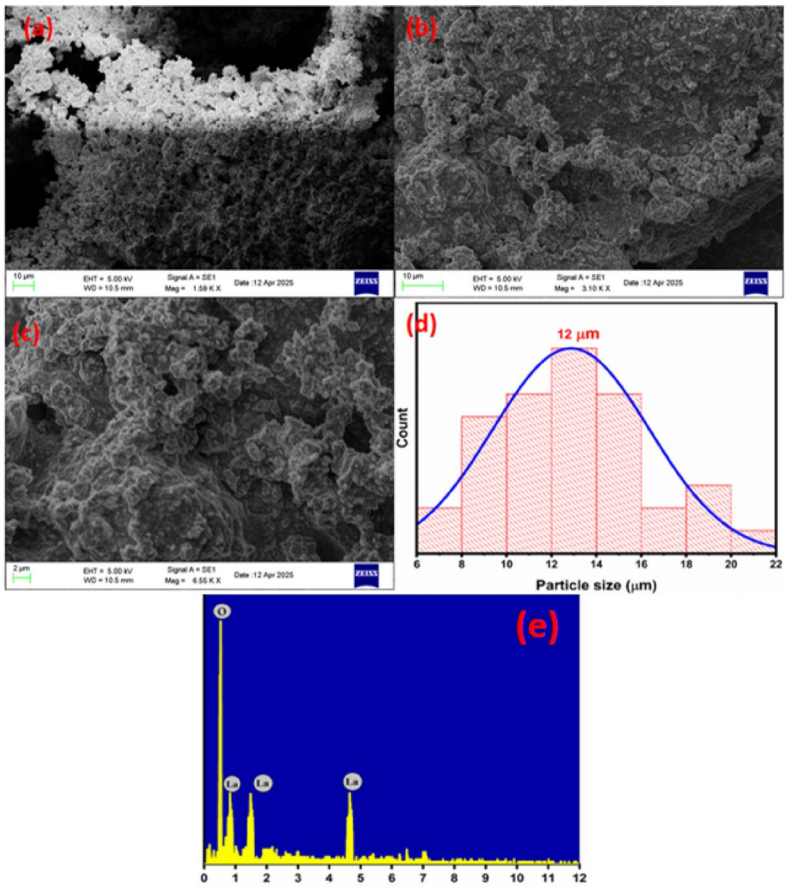

Fig. 6. SEM image, particle size distribution curve, and EDX spectra of La_2O_3.

in Fig. 9. This phenomenon is known as concentration quenching. Figure 8 shows the variation in intensity of peak at the 627 nm, 614 nm, and 587 nm with the concentration of Eu ion in the host lattice.

Concentration quenching phenomenon depends on critical distance (R_c). Critical distance is the distance where the activator ion is close to the optimum distance at specific optimum concentration. Multiple interaction and exchange interaction phenomenon is mainly used for the transfer of energy between the activator ion and the host lattice. Critical distance (R_c) can be approximately calculated by using Blasse's formula[36,37]:

$$R_C = 2\left(\frac{3V}{4\prod X_C N}\right)^{\frac{1}{3}} \tag{1}$$

where V denotes the volume of the unit cell, N denotes the number of cations within the unit cell, and X_c denotes the critical concentration of the activator ion. In the prepared La_2O_3:Eu phosphor, the value of V = 82.2985 Å^3, N = 1, and X_c = 4.0 mol%. By using formula 1 value of R_c is found to be 3.40 which is less than 5 Å. This indicates the quenching phenomenon due to the exchange interaction.

The change in the emission intensity of the prepared phosphor when the level is impacted by the ion interaction and that strength is found by using the equation below. Relation between the intensity and concentration of activator ion can be estimated by using below equation[38].

$$\frac{I}{x} = k[1 + \beta.x^{\frac{\theta}{3}}]^{-1} \tag{2}$$

This equation can be modified as :

$$log\frac{I}{x} = c - \frac{\theta}{3}logx \tag{3}$$

Here k and β are constants with same matrix and excitation condition. Figure 10 show the relationship between Log(I/x) vs Log(x). Slope of Log(I/x) vs log(x) of La_2O_3: Eu^{3+} is 3.127. Slope factor of is found to be 9.381. The value of slope factor is near about 10 so quadrupole–quadrupole interaction is confirmed [39,40].

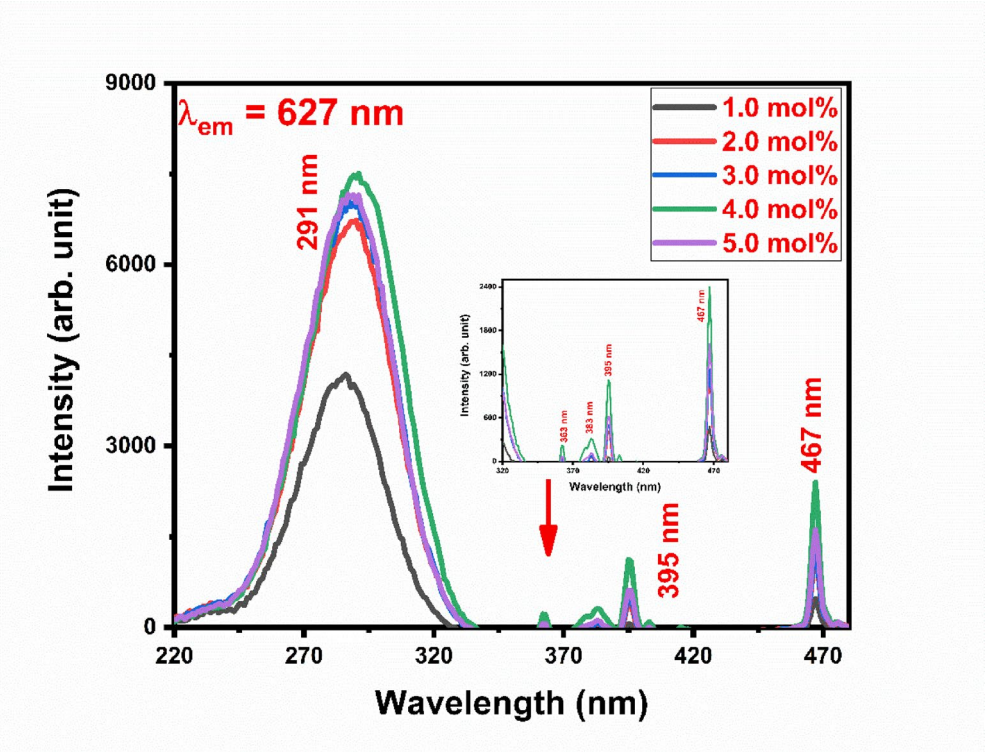

Fig. 7. Excitation spectra of La_2O_3: Eu^{3+} at emission wavelength 627 nm.

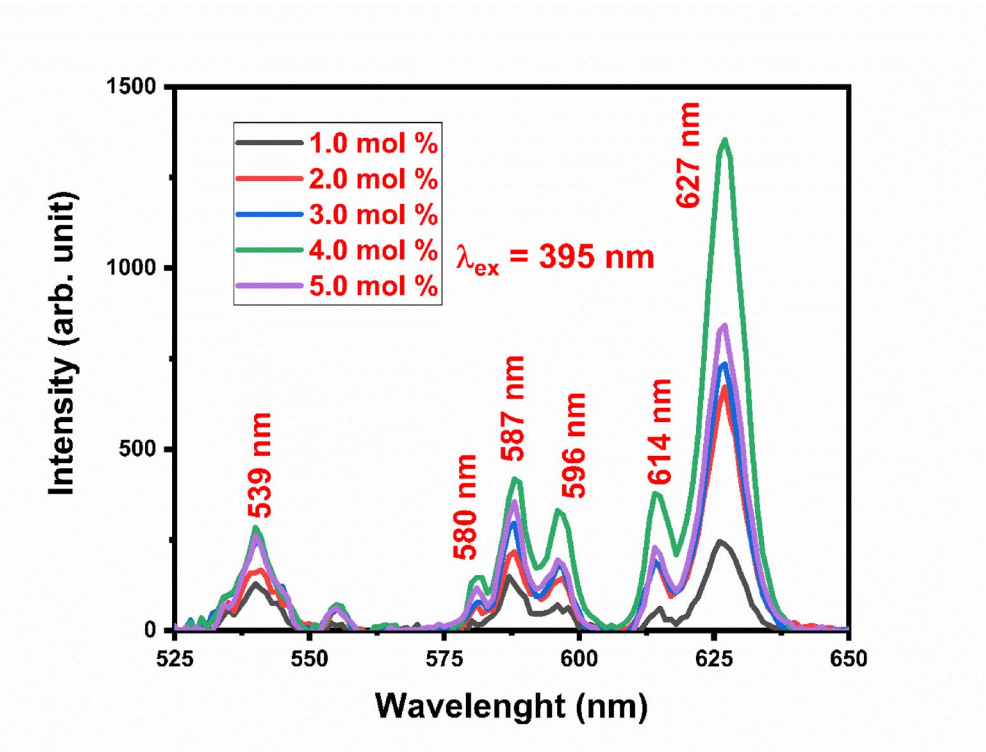

Fig. 8. Emission spectra of La_2O_3: Eu^{3+} at excitation wavelength 395 nm.

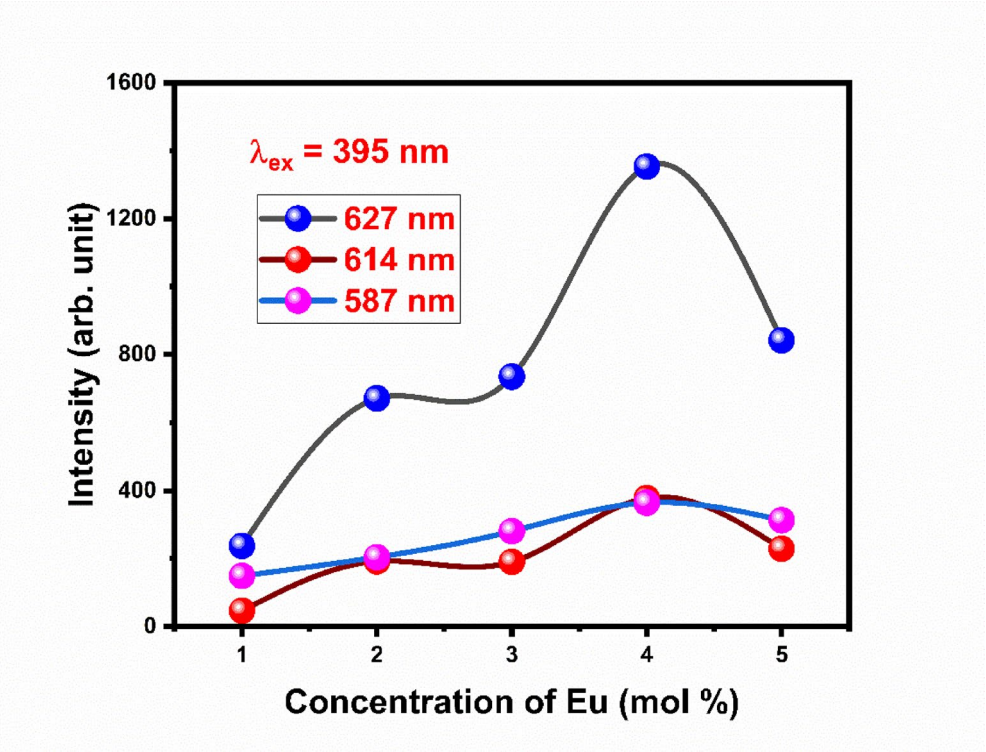

Fig. 9. Concentration quenching of La_2O_3: Eu^{3+}.

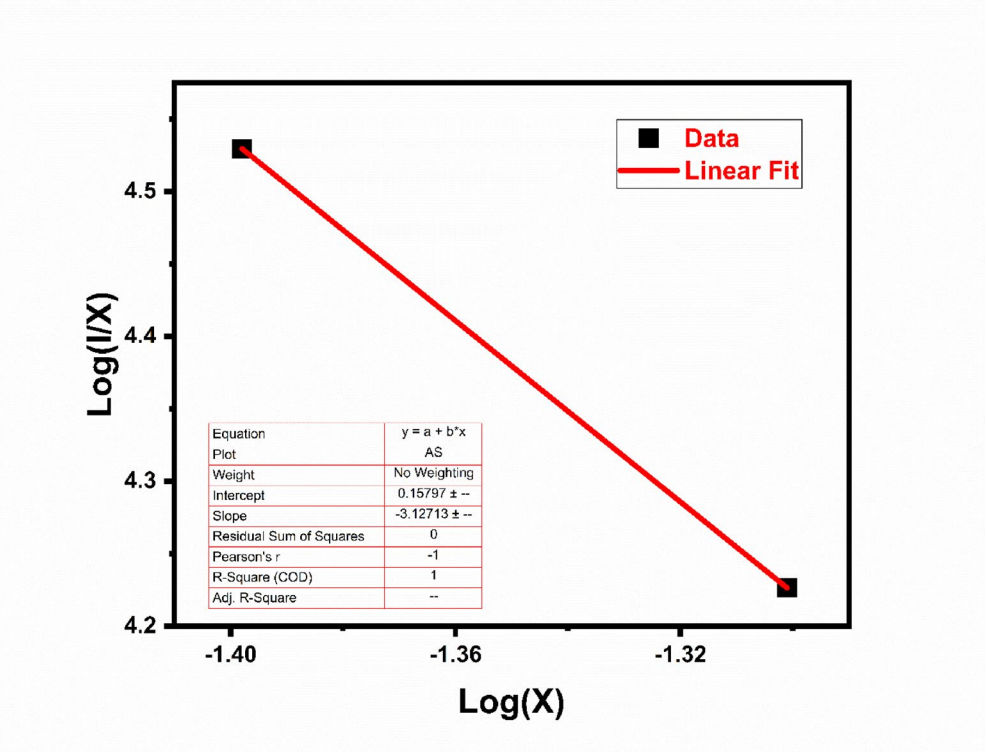

Fig. 10. Log(I/x) vs log(x) of La_2O_3:Eu.

La_2O_3:Ho

Figure 11 shows the excitation spectra of La_2O_3:Ho at emission wavelength of 546 nm recorded from 250 to 400 nm. The emission spectra consist of one major peak at 363 nm and 2 minor peaks at 336 nm, 345 nm. Peak at 363 nm is due to $^5I_8 \rightarrow {}^5G_2, {}^3H_5$ transition while peak at 336 nm, and 345 nm is due to $^5I_8 \rightarrow {}^5G_3$, and $^5I_8 \rightarrow {}^3H_6$ transition respectively[41]. The emission spectra are recorded at the excitation wavelength of 363 nm as shown in Fig. 12. Emission spectra are recorded from 500 to 600 nm of different concentration of Ho^{3+} ions varies from 0.5 mol % to 2.5 mol%. Emission peak consists of one major peak at 546 nm is due to $^5F_4/{}^5S_2 \rightarrow {}^5I_8$ transition. Peak at 546 nm is combine of two sharp peaks. The two closely spaced sharp peaks arise from the transitions between two different energy levels, rather than from crystal defects, since only a single identical crystallographic site is available in the host lattice [42,43]. The two $^5F_4$ and $^5S_2$ excited states of Ho^{3+} are very close in energy, with a separation of about 200–300 cm^{-1}, which is comparable to the phonon energies of oxide hosts (400–600 cm^{-1}). Due to this small gap, lattice vibrations can easily bridge the levels, leading to fast non-radiative thermal coupling between them. Hence, both states remain populated under excitation and take part in the emission process. The radiative transitions from $^5F_4$ and $^5S_2$ to $^5I_8$ the ground state strongly overlap, giving rise to a single broad green band near 546 nm[43,44]. In some high-resolution spectra, a slight asymmetry or weak splitting can be noticed, which further supports the combined contribution of the two levels. As the concentration of Ho^{3+} ion increases from 0.5 mol% to 1.5 mol% intensity increases while after that intensity of emission is decreases gradually until the concentration up to 2.5 mol% Fig. 13. This phenomenon is due to concentration quenching. To find critical distance (R_c) of La_2O_3:Ho, the values of V = 82.2985 $Å^3$, $X_c = 1.5$, and N = 1. By using Eq. 1 the value of R_c is found to be 4.71. The value of which is less than 5 Å, that indicate the quenching phenomenon due to exchange interaction. By using Eq. 3 slope of the Log(I/x) vs log(x) graph (Fig. 14) is 1.74806. The slope factor is 5.24418, which is near to 6 therefore dipole–dipole interaction is confirmed.

La_2O_3:Tm

Figure 15 shows the emission spectra of La_2O_3:Tm at different concentration of Tm^{3+} varies from 0.5 mol % to 2.5 mol%. Emission spectra of La_2O_3:Tm is recorded from 220 to 400 nm at emission wavelength 458 nm. Emission spectra contain one major peak at 237 nm and one minor peak at 361 nm. Broad peak centered at 237 is due to charge transfer between Tm^{3+} to O^{2-}. Peak at 361 nm is due to $^3H_6 \rightarrow {}^1D_2$[29,45].

The emission spectra of La_2O_3:Tm was recorded at the excitation wavelength of 361 nm at different concentration of Tm varying from 0.5 mol % to 2.5 mol % (Fig. 16).The emission spectra of La_2O_3:Tm had one major at 458 nm which is due to the $^1D_2 \rightarrow {}^3F_4$ transition[46,47]. In hexagonal phase there is only one cryptographic site present in lattice, therefore Tm^{3+} ion has to occupy one single site. This results in single emission and narrow peak of emission. Emission peak intensity at 1.5 mol % is the highest among all the concentrations before and after that the intensity of emission spectra decreases. This phenomenon is due the concentration quenching (Fig. 17). Concentration quenching depends on the value of R_c. For La_2O_3:Tm, value N = 1, $X_c = 1.5$, V = 82.2985 $Å^3$. The value of R_c = is found to be 4.71. The value of which is less than 5 Å, that indicate the quenching phenomenon

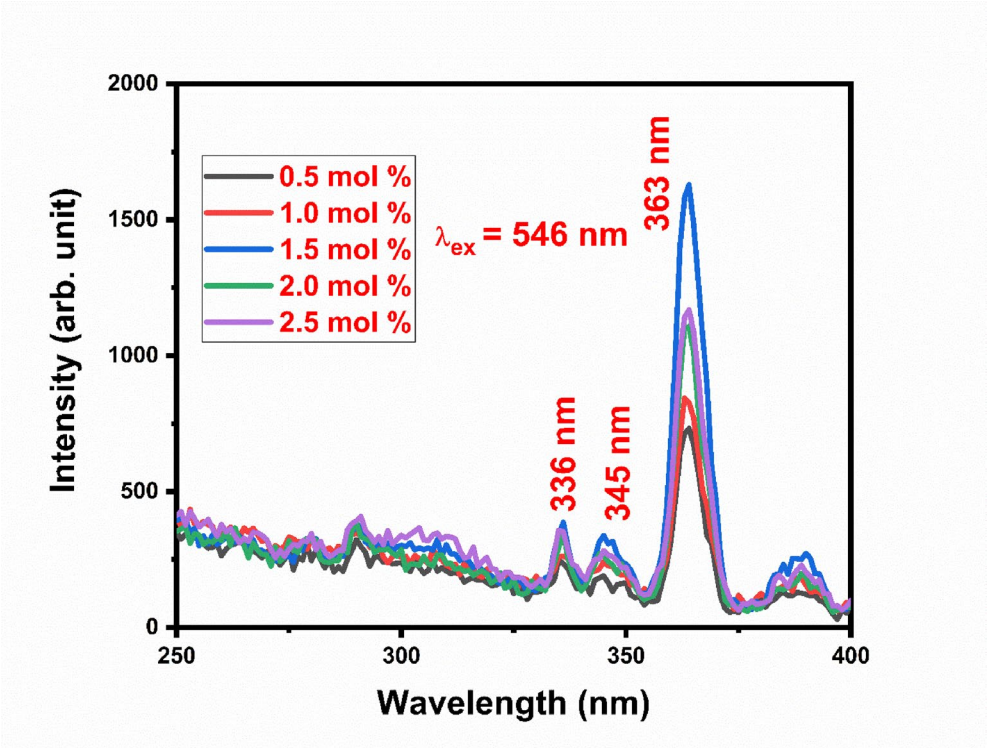

Fig. 11. : Excitation spectra of La_2O_3:Ho at emission wavelength 546 nm.

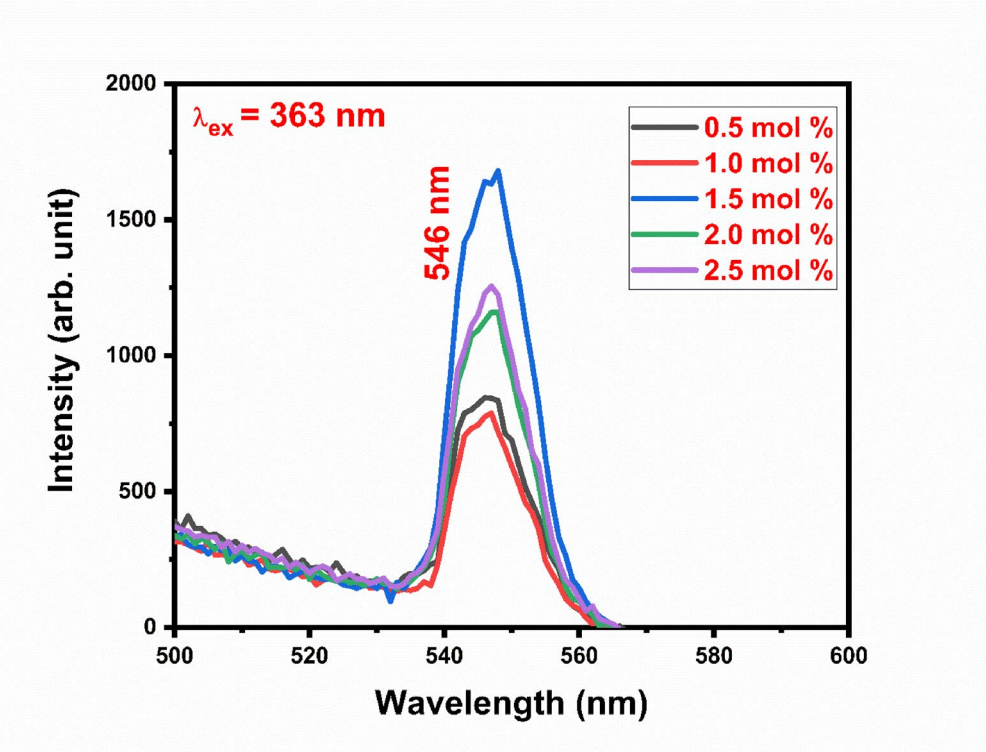

Fig. 12. Emission spectra of La_2O_3:Ho at excitation wavelength 363 nm.

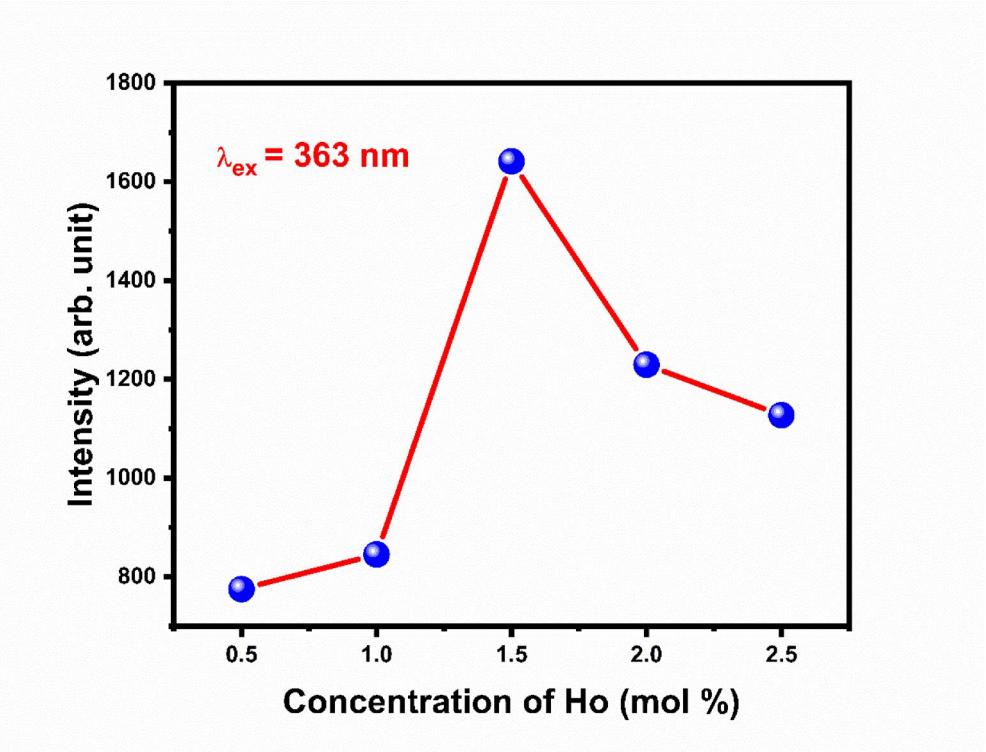

Fig. 13. Variation of intensity with variation of concentration of La_2O_3:Ho.

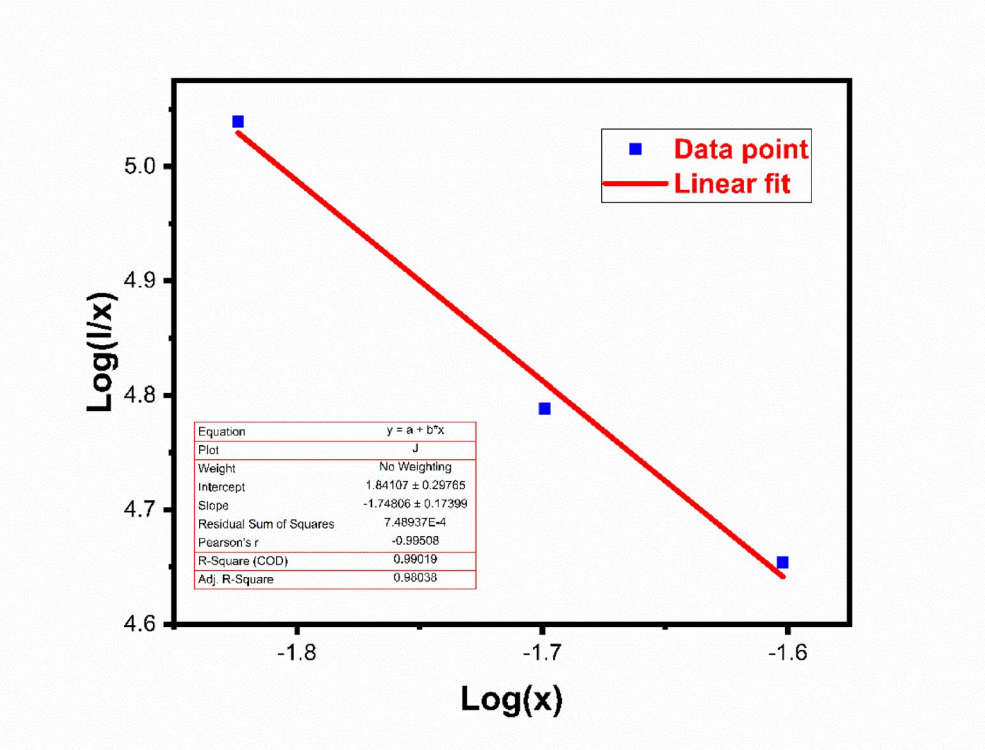

Fig. 14. Log(I/x) vs Log(x) of La_2O_3:Ho.

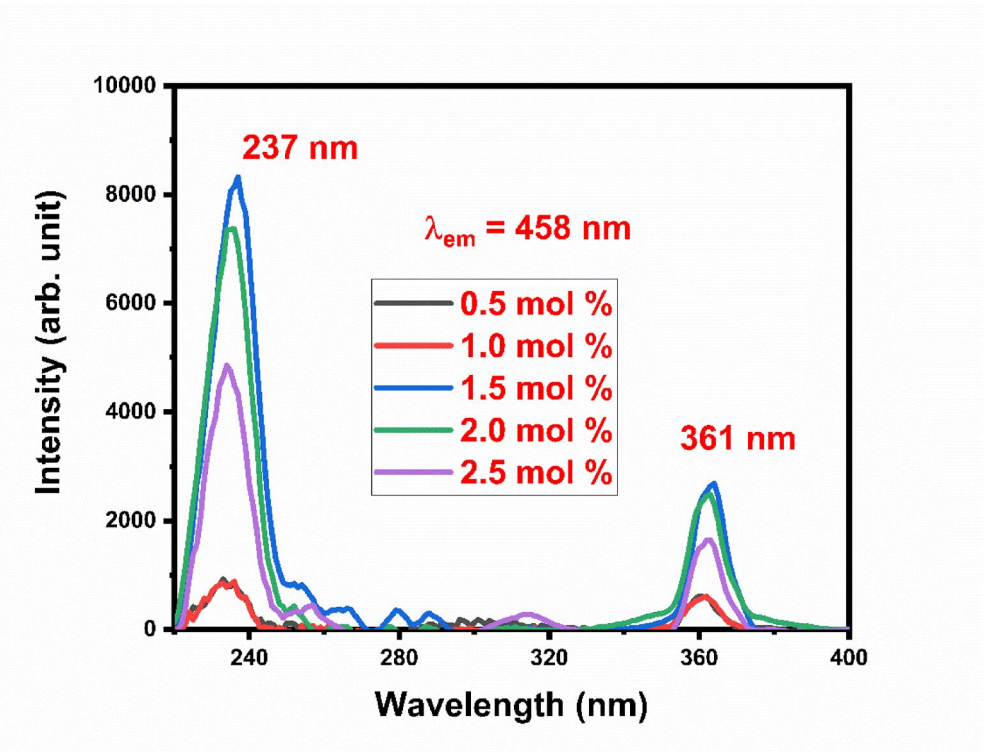

Fig. 15. Excitation spectra of La_2O_3:Tm at emission wavelength 458 nm.

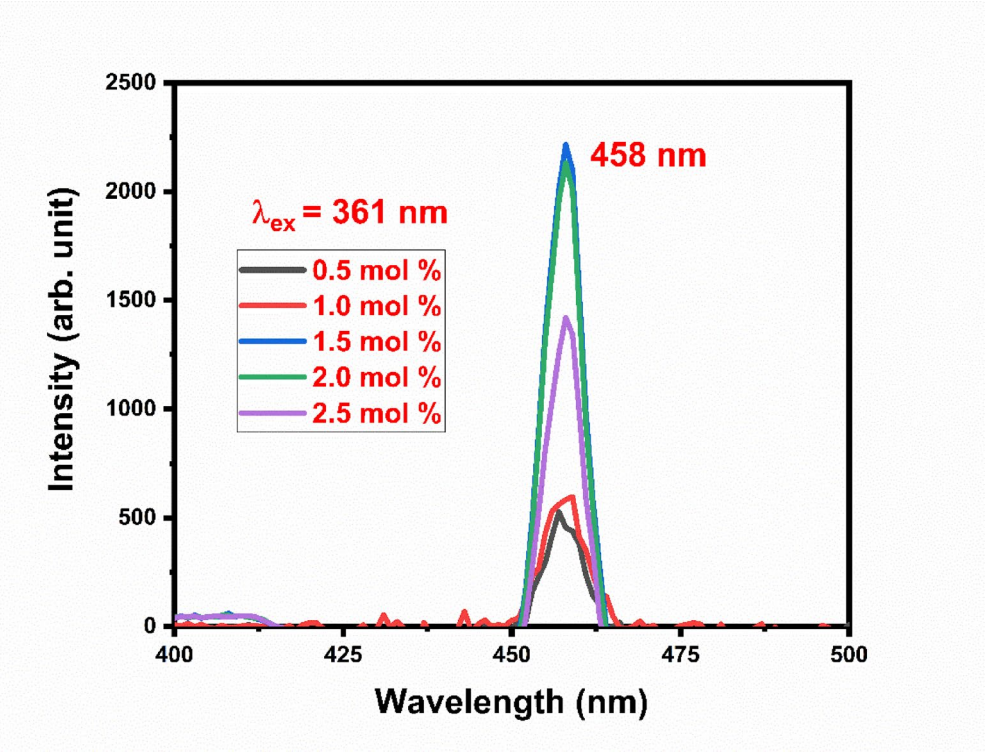

Fig. 16. Emission spectra of La_2O_3:Tm at excitation wavelength 361 nm.

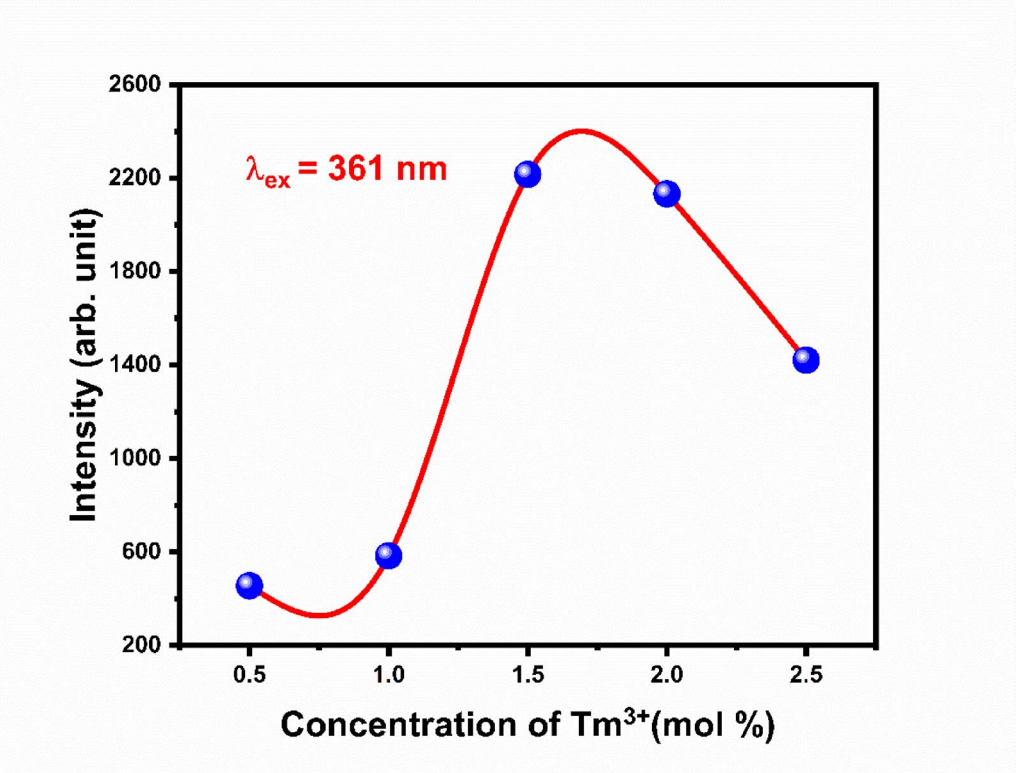

Fig. 17. Variation of intensity with variation of concentration.

due to exchange interaction. By using Eq. 3 slope of Log(I/x) vs log(x) graph (Fig. 18) is 1.74806. The slope factor is 5.502 which is near to 6 therefore dipole–dipole interaction is confirmed.

La_2O_3:Tm/Ho

Figure 19 shows the overlapping spectra of La_2O_3:Tm and La_2O_3:Ho. In Fig. 19 black line indicates the excitation spectra of La_2O_3:Ho at emission wavelength of 546 nm, while red line indicates the excitation spectra La_2O_3:Tm at emission wavelength 458 nm. In the overlapping spectra, both excitation spectra are overlapped at two points at 306 nm and 361 nm. Broad peaks from 280 to 340 nm centered at 306 nm are observed only in the co-doped phosphor excitation spectra as compared to single doped phosphor. In the Fig. 19, the excitation-excitation overlap occurred. So, energy transfer is from lower wavelength (458 nm) of Tm^{3+} ion to higher wavelength (546 nm) of Ho^{3+} ion. To study the energy transfer between them we keep the lower wavelength ion (Tm) is constant at 1.5 mol% where the concentration quenching is happens. The concentration of higher wavelength ion (Ho^{3+}) varies from 0.5 mol% to 2.5 mol%. So, to study the energy transfer in La_2O_3:Tm/Ho we recorded the emission spectra at 306 nm and 361 nm.

The emission spectra of La_2O_3:Tm/Ho is shown in the Fig. 20 at the excitation wavelength of 361 nm. The emission spectra of La_2O_3:Tm/Ho contains major 2 peaks at 458 nm and 547 nm. The peaks at 458 nm and 547 nm are due to $^1D_2 \rightarrow {}^3F_4$ and $^5F_4/^5S_2 \rightarrow {}^5I_8$ transitions, respectively. As the concentration of Ho^{3+} ion increases from 0.5 mol% to 2.5 mol%, the emission intensity of peak at 458 nm (Tm^{3+}) ion decreases. The emission intensity of Ho^{3+} ion increases gradually. The decrease in energy is due to the transfer of the energy from Tm^{3+} ion Tm^{3+} ion to the Ho^{3+} ion in the host lattice. This variation of emission intensity in specific manner concludes that the energy transfer in La_2O_3:Tm/Ho has occurred. The variation of intensity is shown in the Fig. 21. Energy transfer efficiency can be find using following equation:

$$\eta_T = 1 - \frac{I_a}{I_{ao}} * 100\% \tag{4}$$

where I_a is intensity of the acceptor atom and I_{ao} is intensity of acceptor ion without donor atom. In the above case, energy transfer happens from the Tm ion to the Ho ion, so Ho is the acceptor ion while Tm is donor atom. Energy transfer is ranges from 8.18809 to 54.52997%. As increasing the concentration of Ho ion efficiency start decreases as shown in Table 5.

Figure 22 shows the emission spectra of La_2O_3:Tm/Ho at excitation wavelength 306 nm. Emission spectra contain one broad peak from 410 to 530 nm humped at 450 nm and 474 nm, while one sharp peak at 546 nm. Broad peak is humped at 450 and 474 nm is due to $^1D_2 \rightarrow {}^3F_4$ transition while the peak at 546 nm is due to $^5F_4/^5S_2 \rightarrow {}^5I_8$ transition of Ho^{3+} ion. Intensity of both broad and sharp peak increases as their increase in the concentration of Ho^{3+} ion in host lattice. The phenomenon of energy transfer does not manifest in that specific

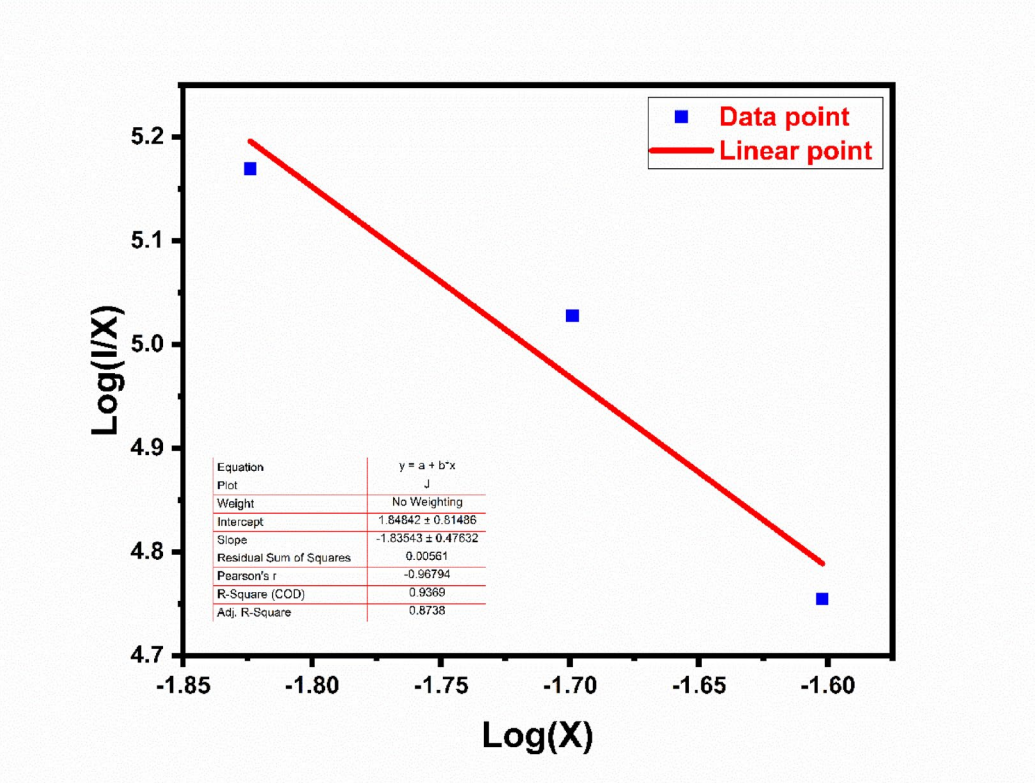

Fig. 18. Log(I/x) vs Log(x) of La_2O_3:Tm.

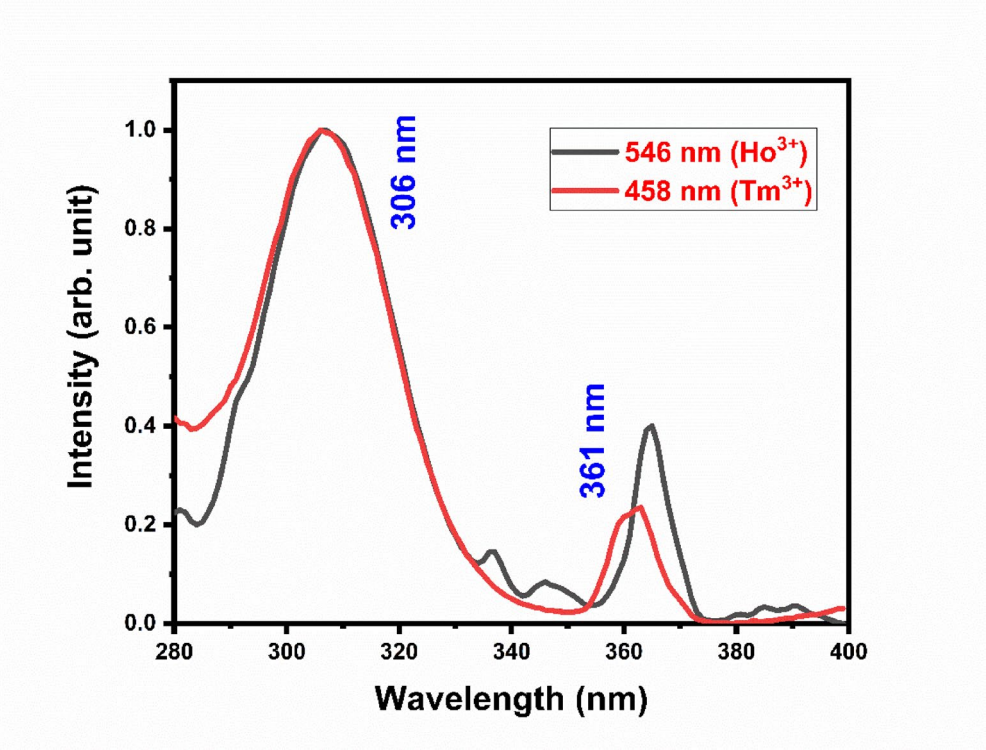

Fig. 19. Overlap graph of La_2O_3:Tm/Ho.

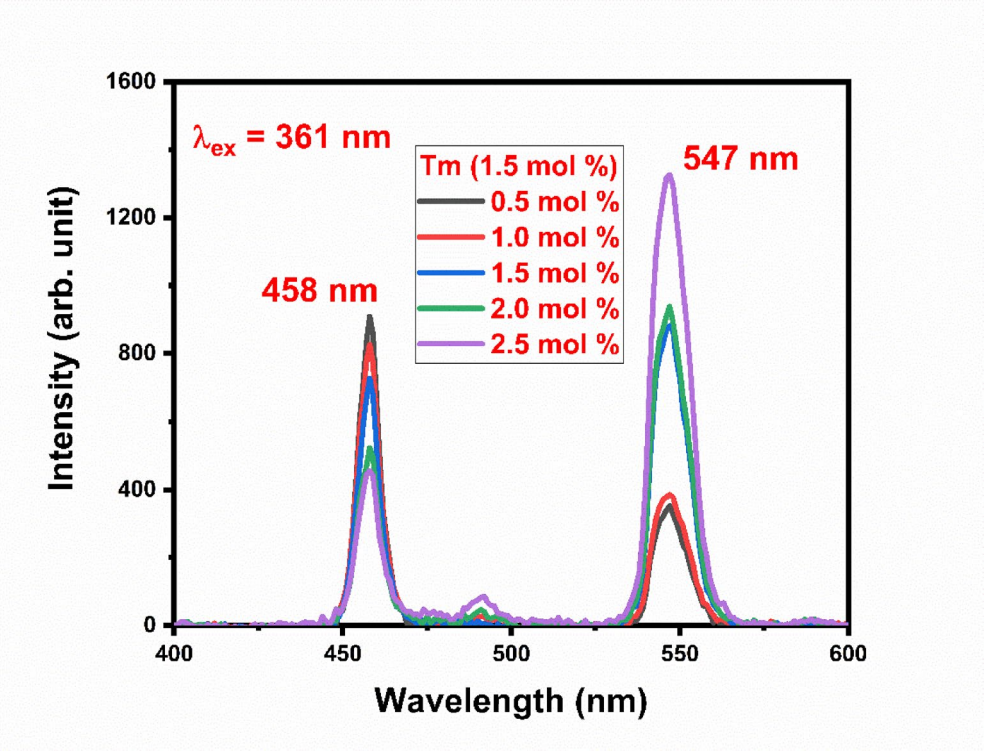

Fig. 20. Emission spectra of La_2O_3:Tm/Ho at excitation wavelength 361 nm.

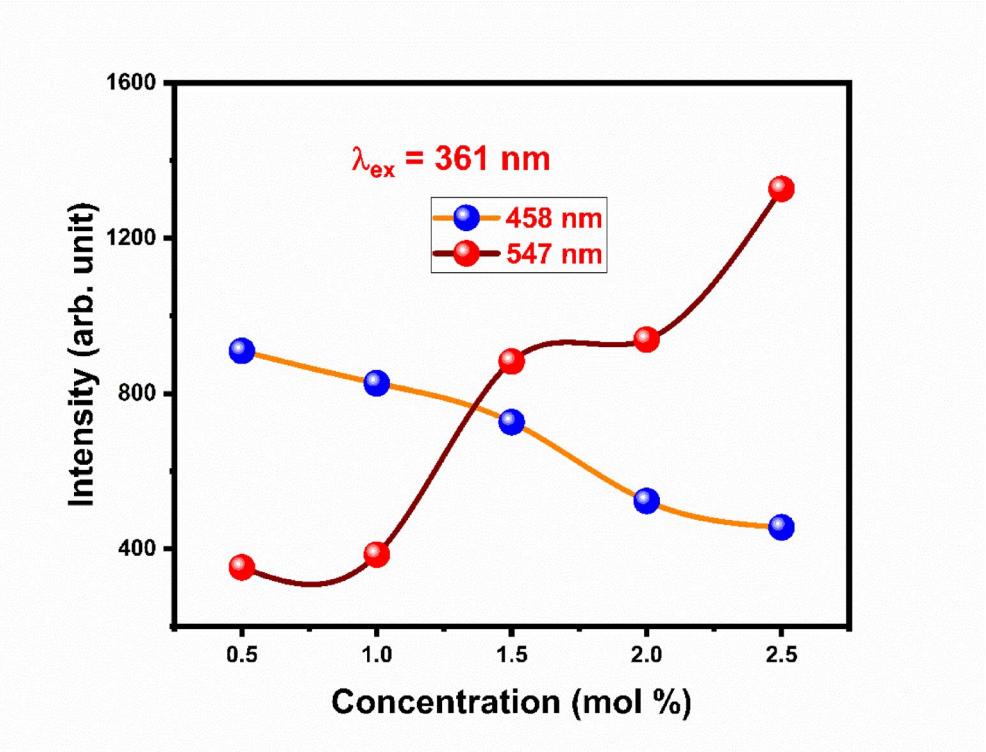

Fig. 21. variation of intensity in La_2O_3:Tm/Ho at excitation wavelength 361 nm.

sr	Name	I_{Er}	I_{Ero}	Efficiency (%)
1	La_2O_3: Tm^{3+}(1.5 mol%)/Ho^{3+}(0.5 mol%)	775.1	352.4382	54.52997
2	La_2O_3: Tm^{3+}(1.5 mol%)/Ho^{3+}(1.0 mol%)	845.526	385.25	54.43665
3	La_2O_3: Tm^{3+}(1.5 mol%)/Ho^{3+}(1.5 mol%)	1641.372	882.05	46.26142
4	La_2O_3: Tm^{3+}(1.5 mol%)/Ho^{3+}(2.0 mol%)	1229.488	938.538	23.66432
5	La_2O_3: Tm^{3+}(1.5 mol%)/Ho^{3+}(2.5 mol%)	1227.368	1126.87	8.18809

Table 5. Energy transfer efficiency of La_2O_3: Tm^{3+}/Ho^{3+}

emission spectra. In emission spectra at excitation wavelength 306 nm, it has anomalous behavior compared to that of emission spectra at 361 nm.

Two different types of emission at different excitation in same host lattice is due to the difference in energy transfer and energy absorption mechanism. Excitation at 361 nm is directly resembles to the $^3H_6 \rightarrow {}^1D_2$ transition of Tm^{3+} ion, this populates the excitation states and resultant gives blue emission at 458 nm ($^1G_4 \rightarrow {}^3H_6$), by ion-ion cross-relaxation phenomenon. The energy from Tm^{3+} ion is transfer to the Ho^{3+} ion. Transfer of energy give sharp peak at 547 nm due to transition $^5S_2 \rightarrow {}^5I_8$. When we excite the La_2O_3:Tm/Ho with excitation wavelength 306 nm , absorption of high energy emerges primarily from the host lattice not dopant ions(Tm^{3+},Ho^{3+}). Host lattice absorbs the energy by storing energy in broad electron–hole pair or in charge transfer state. Ho^{3+} ion act as high and efficient trap for mobile energy due to its high optimal energetic alignment with high-lying Ho^{3+} energy levels like ^5G. This high energy absorption leads to where instance host-ion transfer overpopulate the $^5S_2$ state of Ho^{3+} ion, which result in the occurrence of intense and sharp emission at 546 nm is observed. The process of recombination of energy in Ho ion is so fast so that Tm^{3+} quenches its luminescence. Broad spectra is due to self emission of host lattice due to host lattice defect. Humped broad background from 410–530 nm represents only the small fraction of exactions that recombine radioactively at defect sites before being captured by Ho^{3+}.

La_2O_3:Ho/Eu

Figure 23 shows the overlap spectra of La_2O_3:Ho/Eu. In Fig. 23 black line indicate the excitation spectra La_2O_3:Eu at emission wavelength 616 nm, while red line indicates excitation spectra of La_2O_3:Ho at emission spectra 545 nm. Both spectra overlap at 2 points in near UV region. In He, excitation-excitation overlaps happen. To study the energy transfer between these ions, we keep the lower wavelength (545 nm) constant at 1.5 mol%, where the quenching occurs. Keep varying the concentration of higher wavelength (616 nm) of Eu^{3+} ion.

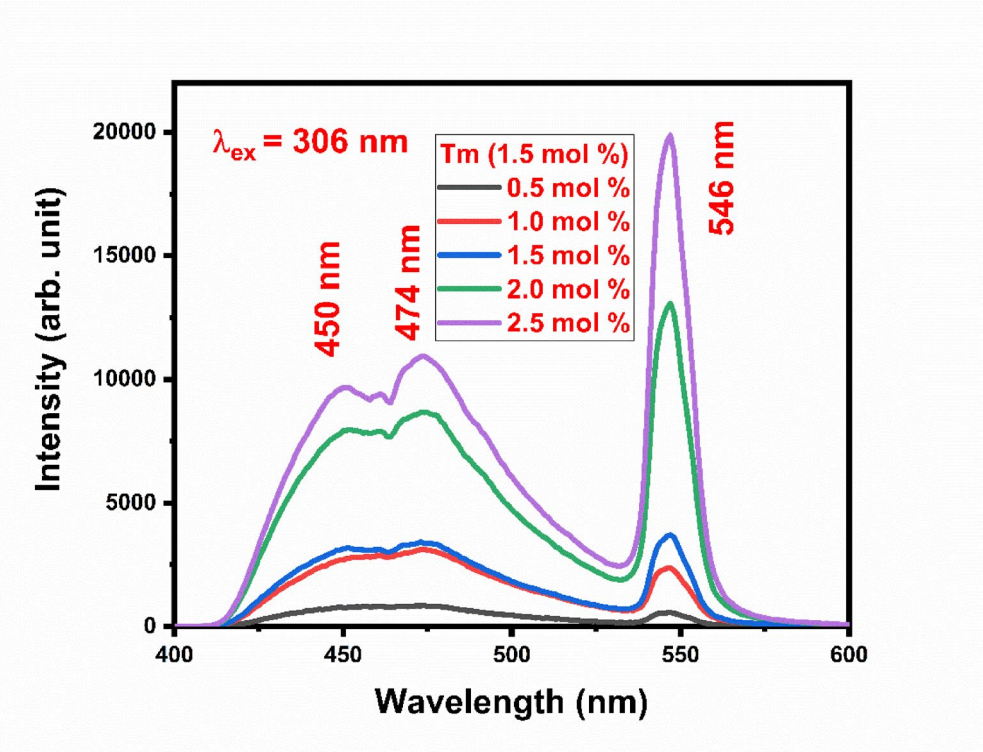

Fig. 22. Emission spectra of La_2O_3:Tm/Ho at excitation wavelength 306 nm .

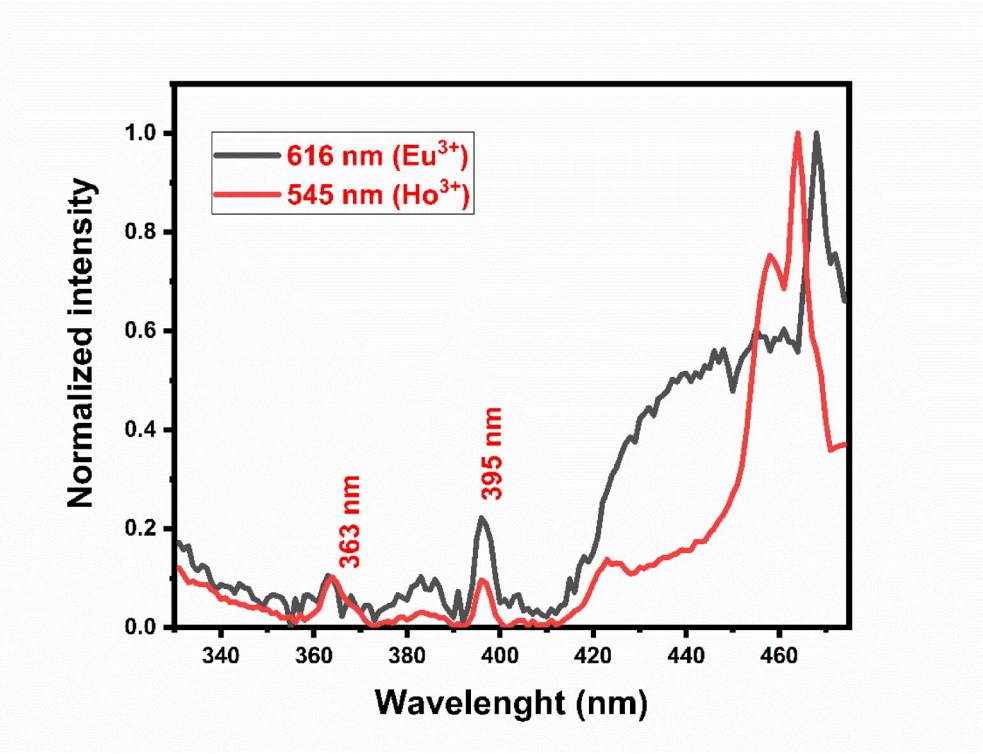

Fig. 23. : Overlap Spectra of La_2O_3:Ho/Eu.

Emission spectra of La_2O_3:Ho/Eu is recorded at excitation wavelength 363 nm is shown in Fig. 24. Emission spectra of La_2O_3:Ho/Eu contain one major peak at 545 nm and some minor peaks at 587 nm, 596 nm, 613 nm, and 626 nm. Peak at 545 nm is due to the transition of Ho ion due to $^5F_4$ /$^5S_2 \rightarrow {}^5I_8$ transition. Peak at 587 nm, and 596 nm, 613 nm, and 626 nm are due to $5D_0 \rightarrow 7F_0$, $5D_0 \rightarrow 7F_1$ transition of Eu^{3+} ion respectively. As the concentration of Eu^{3+} increases, the intensity of the Ho^{3+} emission peak at 545 nm decreases, while the intensities of the Eu^{3+} emission peaks at 587 nm, 596 nm, 613 nm, and 626 nm increase (Fig. 25). That conclude the energy transfer in La_2O_3:Ho/Eu has occurred. Energy transfer efficiency of La_2O_3:Ho/Eu is calculate using Eq. 4 and shown in the Table 6. Acceptor ion is Eu and donor atom is Ho. Maximum energy transfer happens at La_2O_3:Ho^{3+}(1.5 mol%)/Eu^{3+}(2.0 mol%) with efficiency of 93.75481%.

La_2O_3:Tm/Eu

In Fig. 26 shows the overlap spectra of La_2O_3:Tm/Eu. In Fig. 26 black line shows the excitation spectra of La_2O_3:Tm at emission wavelength 458 nm, while red line shows the excitation spectra LE at emission wavelength 627 nm. Both spectra are overlap at 362 nm. In excitation-excitation overlap spectra, we keep lower wavelength constant (Tm) at quenching concentration, while higher wavelength (Eu) is varying.

Figure 27 shows the emission spectra La_2O_3:Tm at excitation wavelength 362 nm. Emission spectra of La_2O_3:Tm/Eu contain one major peak at 458 nm and minor peaks at 540 nm, 588 nm, 615 nm, and 627 nm. Peak at 458 nm, 540 nm, 588 nm, 615 nm, and 627 nm is due $^1D_2 \rightarrow {}^3F_4$ $5D_0 \rightarrow 7F_0$, $5D_0 \rightarrow 7F_1$ transition. As the concentration of Eu ion increases from 1 mol% to 5 mol% intensity of peak at 458 nm due to Tm transition decreases. As increasing the concentration of Eu ion increases, the intensity of peak due to the Eu transition is increases as shown in Fig. 28. This is concluded that energy transfer has occurred. The intensity of the Tm peak is significantly higher compared to that of the Eu ions. Under 362 nm excitation, Tm ions strongly absorb and predominantly radiates intense blue light, while transferring only a small fraction of energy to Eu ions. This limited energy transfer results in the observed difference in emission intensities. Table 7 shows calculated energy transfer efficiency using Eq. 4 of La_2O_3:Tm/Eu. In above case donor atom is Tm and acceptor ion is Eu. Energy transfer efficiency varies from 90.70919 to 75.60775% with maximum at La_2O_3:Tm^{3+}(1.5 mol%)/Eu^{3+}(1.0 mol%).

La_2O_3:Tm/Ho/Eu

In the preceding study we analyzed the energy transfer between the La_2O_3:Tm/Ho/Eu, La_2O_3:Tm/Ho, and La_2O_3:Tm/Eu. To achieve the complete WLEDs phosphor with high red color component. We synthesis the triple dope phosphor in same host. Figure 29 shows the overlap spectra of the at excitation wavelength of La_2O_3:Tm/Ho/Eu. Above Fig. 29 has 3 excitation spectra at 3 different emission wavelengths. Emission wavelength at 616 nm, 545 nm, and 458 nm is associated with the Eu^{3+}, Ho^{3+}, and Tm^{3+} ion excitation. All excitation spectra are overlap at 363 nm. To study the triple doped phosphor, we keep the concentration of Tm and Ho ion constant at 1.5 mol% each. This concentration has balaced components of both blue and green colour which is very essential to achieve WLEDs phosphor.The concentration of Eu^{3+} ion is changes from 1.0 mol% to 5 mol%.

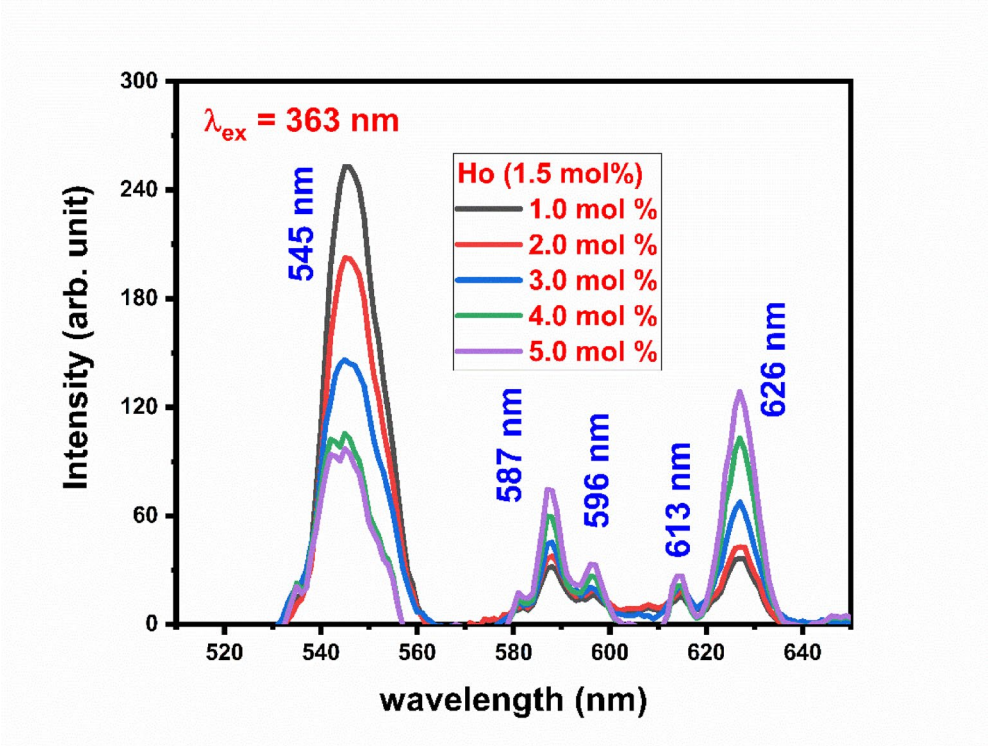

Fig. 24. Emission spectra of La_2O_3:Ho/Eu at excitation wavelength 363 nm.

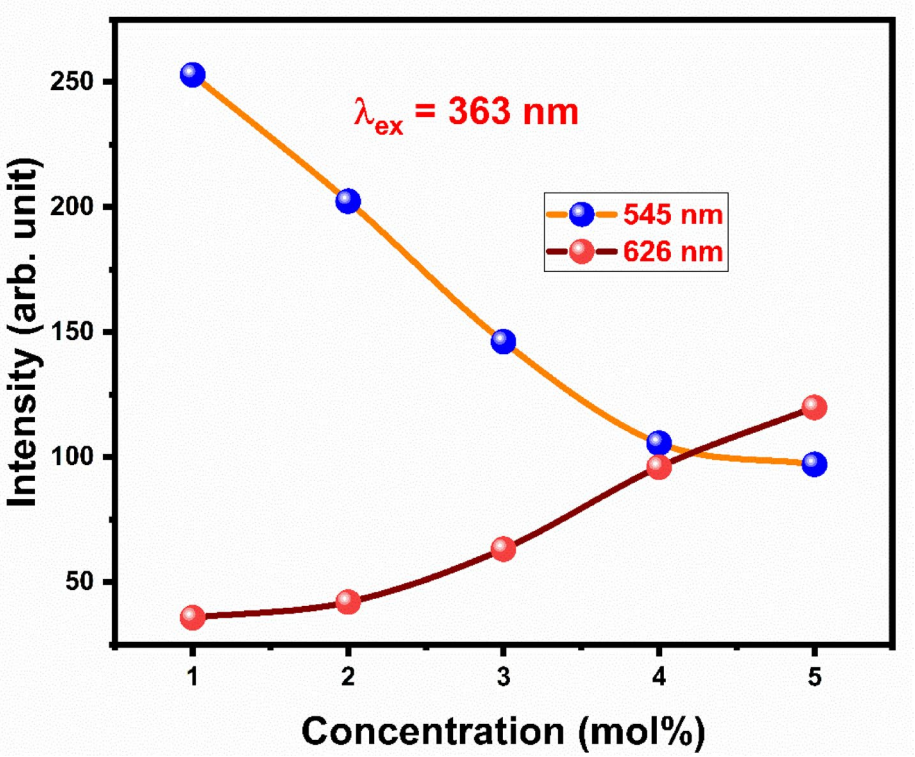

Fig. 25. : variation of intensity in La_2O_3:Ho/Eu at excitation wavelength 361 nm.

Sr	Name	I_{Er}	I_{Ero}	Efficiency (%)
1	La_2O_3: Ho^{3+}(1.5 mol%)/Eu^{3+}(1.0 mol%)	237.6543	35.6527	84.99808
2	La_2O_3: Ho^{3+}(1.5 mol%)/Eu^{3+}(2.0 mol%)	671.6266	41.94435	93.75481
3	La_2O_3: Ho^{3+}(1.5 mol%)/Eu^{3+}(3.0 mol%)	735.1859	63.17407	91.40706
4	La_2O_3: Ho^{3+}(1.5 mol%)/Eu^{3+}(4.0 mol%)	1353.832	95.87116	92.91853
5	La_2O_3: Ho^{3+}(1.5 mol%)/Eu^{3+}(5.0 mol%)	842.2185	119.839	85.77104

Table 6. Energy transfer efficiency of La_2O_3: Ho^{3+}/Eu^{3+}

Figure 30 shows the excitation spectra of La_2O_3:Tm/Ho/Eu at excitation wavelength 363 nm. Emission spectra contain majorly 4 peaks. One peak in blue region at 459 nm, second in green region at 547 nm, nest at 587 nm in orange region, while last peak at 627 nm is in red region. Peaks at 459 nm, 547 nm, 587 nm, and 627 nm are associate with $^1D_2 \rightarrow {}^3F_4$,$^5F_4/^5S_2 \rightarrow {}^5I_8$, $5D_0 \rightarrow 7F_0$, and $5D_0 \rightarrow 7F_1$ transition, respectively. As we increase the concentration of Eu^{3+} ion, intensity peaks at 459 nm, and 547 nm decreases continuously, while the intensity of peak at 587 nm, and 627 nm due to Eu^{3+} ion increases continuously. Detailed energy transfer is shown in Fig. 31. Table 8 shows the energy transfer efficiency of La_2O_3:Tm/Ho/Eu with maximum at La_2O_3: Tm^{3+}(1.5 mol%)/ Ho^{3+}(1.0 mol%)/Eu^{3+}(2.0 mol%) about 77.2498% calculated using Eq. 4. High charge carrier mobility can be achieved by properly designing the material, adding suitable dopants, and optimizing the crystal structure. By reducing the charge recombination loss leads to efficient energy transfer in the phosphor[48] .

CIE analysis

Parameters of emission of phosphor can be analyzed using Commission de I Eclairage (CIE) coordinates. CIE coordinates are giving the theoretical color of emission in CIE diagram. CIE co-ordinates are also used to find the color purity and CCT (Color co-related temperature) of prepared phosphor. Color purity of prepared sample is calculated by using following equation[49]:

$$Colorpurity = \frac{\sqrt{(X - X_i)^2 + (Y - Y_i)^2}}{\sqrt{(X_d - X_i)^2 + (Y_d - Y_i)^2}} * 100\% \quad (5)$$

where, (X, Y) are CIE chromaticity co-ordinate, (Xi, Yi) are co-ordinate of white perfect light and (Xd, Yd) is co-ordinate of dominant wavelength. Value (Xi, Yi) used in calculation are (0.33, 0.33). Color co-related temperature of phosphor can be calculated by using formula [24]:

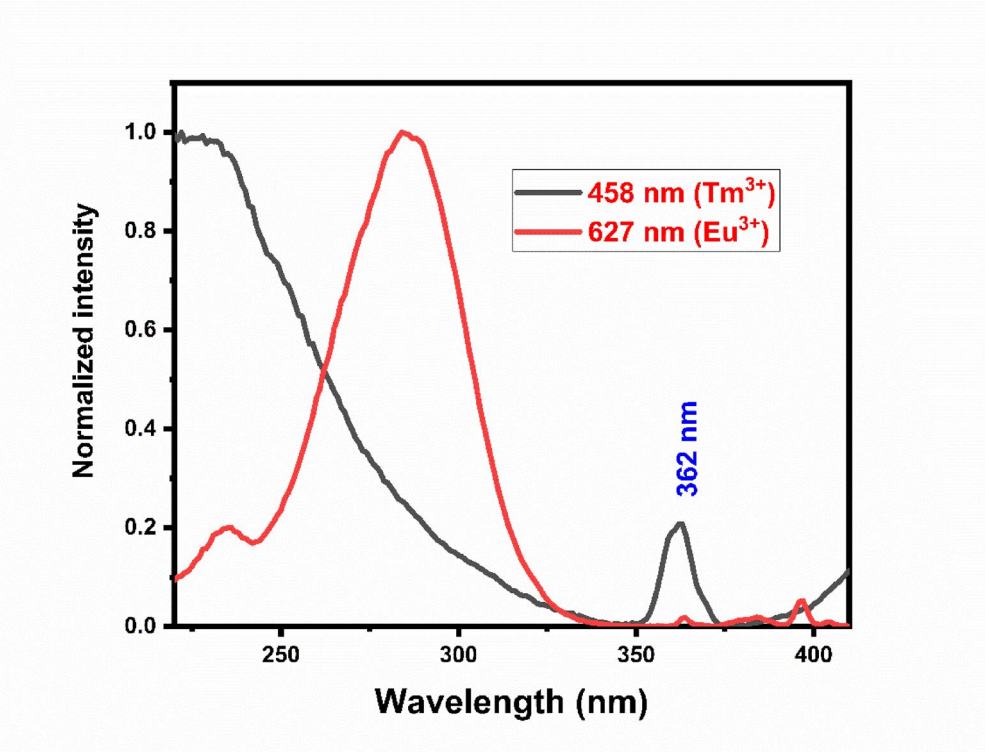

Fig. 26. Overlap spectra of La_2O_3:Tm/Eu.

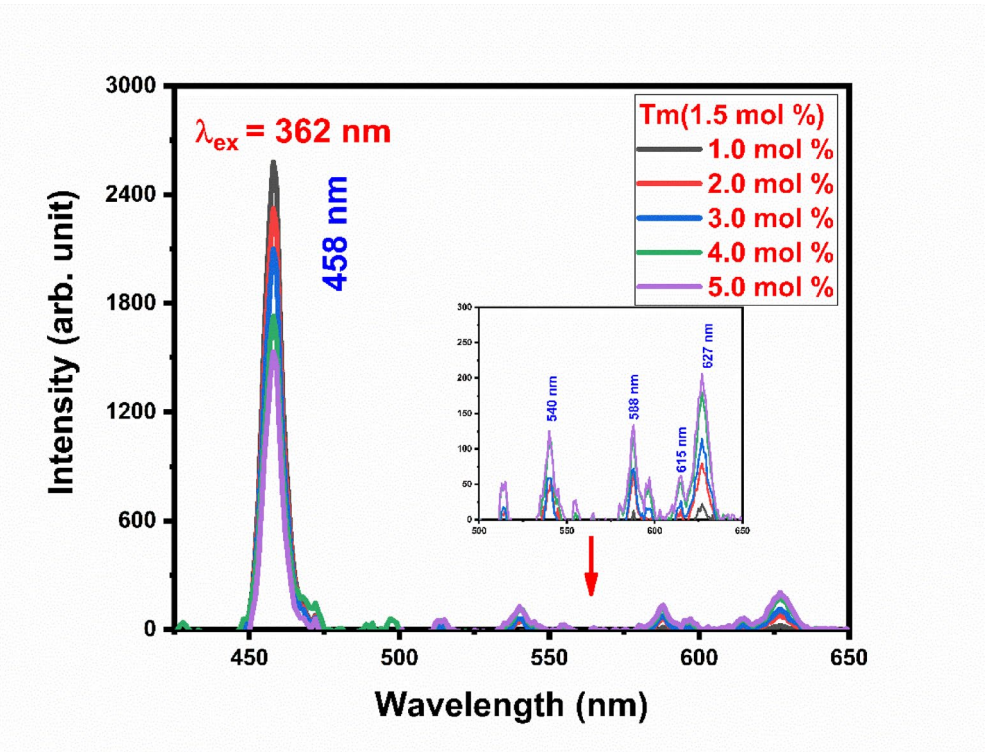

Fig. 27. Emission spectra of La_2O_3:Tm/Eu at excitation wavelength 362 nm.

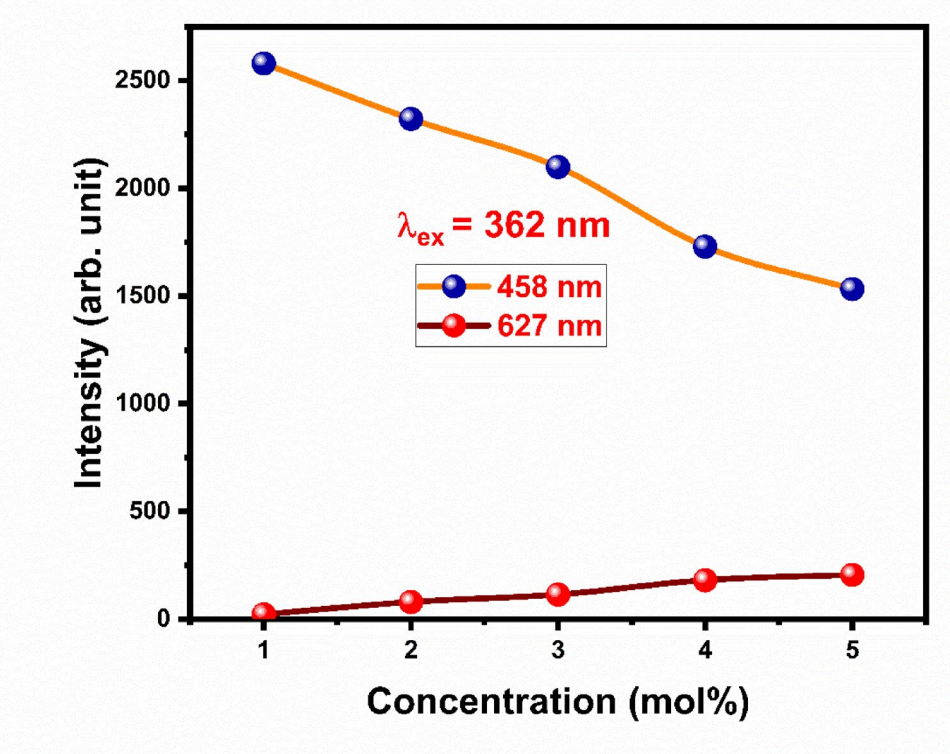

Fig. 28. variation of intensity in La_2O_3:Tm/Eu at excitation wavelength 361 nm.

sr	Name	I_{Er}	I_{Ero}	Efficiency (%)
1	La_2O_3:Tm^{3+}(1.5 mol%)/Eu^{3+}(1.0 mol%)	237.6543	22.08	90.70919
2	La_2O_3: Tm^{3+}(1.5 mol%)/Eu^{3+}(2.0 mol%)	671.6266	79.626	88.1443
3	La_2O_3: Tm^{3+}(1.5 mol%)/Eu^{3+}(3.0 mol%)	735.1859	113.942	84.50161
4	La_2O_3: Tm^{3+}(1.5 mol%)/Eu^{3+}(4.0 mol%)	1353.832	180.228	86.68757
5	La_2O_3: Tm^{3+}(1.5 mol%)/Eu^{3+}(5.0 mol%)	842.2185	205.436	75.60775

Table 7. Energy transfer efficiency of La_2O_3: Tm^{3+}/Eu^{3+}

$$CCT = -437n^3 + 3601n^2 + -6861n + 5514.31 \ldots.(6).$$

La_2O_3:Eu

Figure 32 shows the CIE diagram of La_2O_3:Eu. CIE co-ordinates are in red region that confirm the emission of red color phosphor. As the concentration of Eu^{3+} ion increases from 1.0 mol% to 5 mol%, CIE coordinates shift from orange-red region to red region in CIE diagram. Table 9 shows the CIE coordinate, color purity and CCT of prepared sample. La_2O_3:Eu^{3+}(1.0 mol%) and La_2O_3:Eu^{3+}(2.0 mol%) shows the orange-red emission with moderate colour purity , that makes it more prominent candidate for display coating, decorative lighting. La_2O_3:Eu^{3+}(3.0 mol%) and La_2O_3:Eu^{3+}(4.0 mol%) has intense red emission with high colour purity (more than 80%) therefore this phosphor can be efficacious for solid-state lighting, display backlighting, phosphor-converted LEDs. Quenching in colour purity happens at La_2O_3:Eu^{3+}(5.0 mol%) concentration still greater than 80%. La_2O_3:Eu^{3+}(5.0 mol%) can be used for solid-state lighting, display backlighting, phosphor-converted LEDs.

La_2O_3:Ho

Figure 33 shows the CIE co-ordinate of La_2O_3:Ho. In CIE diagram the coordinates are in green region that confirm the emission in green region. Table 10 shows the CIE co-ordinate, color purity and CCT of prepared sample. La_2O_3:Ho^{3+} phosphor has high intense green emission with high colour purity ranging from 96% to 98.98%. La_2O_3:Ho^{3+} phosphor has narrow and single peak emission that makes it more useful in green LEDs phosphor, leaser. La_2O_3:Ho^{3+}(0.5 mol%) and La_2O_3:Ho^{3+}(1.0 mol%) has high CCT around 7300 with stable and intense green emission which makes it more prominent in display coatings and decorative lighting. La_2O_3:Ho^{3+}(1.5 mol%) and La_2O_3:Ho^{3+}(2.0 mol%) has improvement in colour purity till 98.98% with decreases in CCT so this phosphor have applications in solid-state lighting, laser applications, and optical devices. La_2O_3:Ho^{3+}(2.5 mol%) has decreases in colour purity and stable CCT.

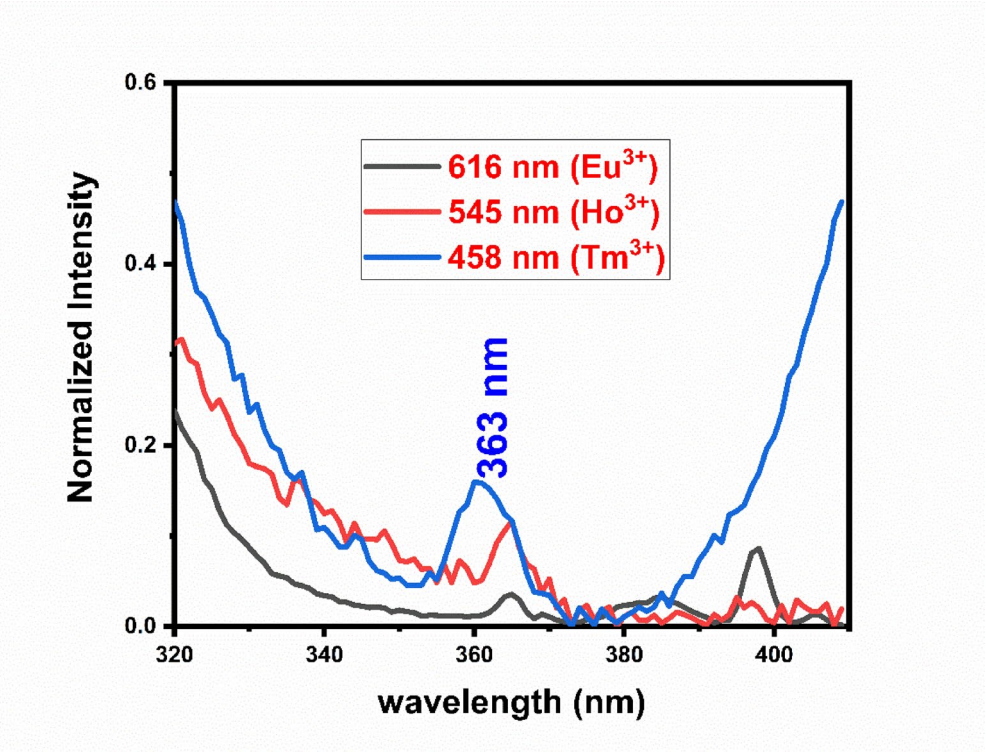

Fig. 29. Overlap spectra of La_2O_3:Tm/Ho/Eu.

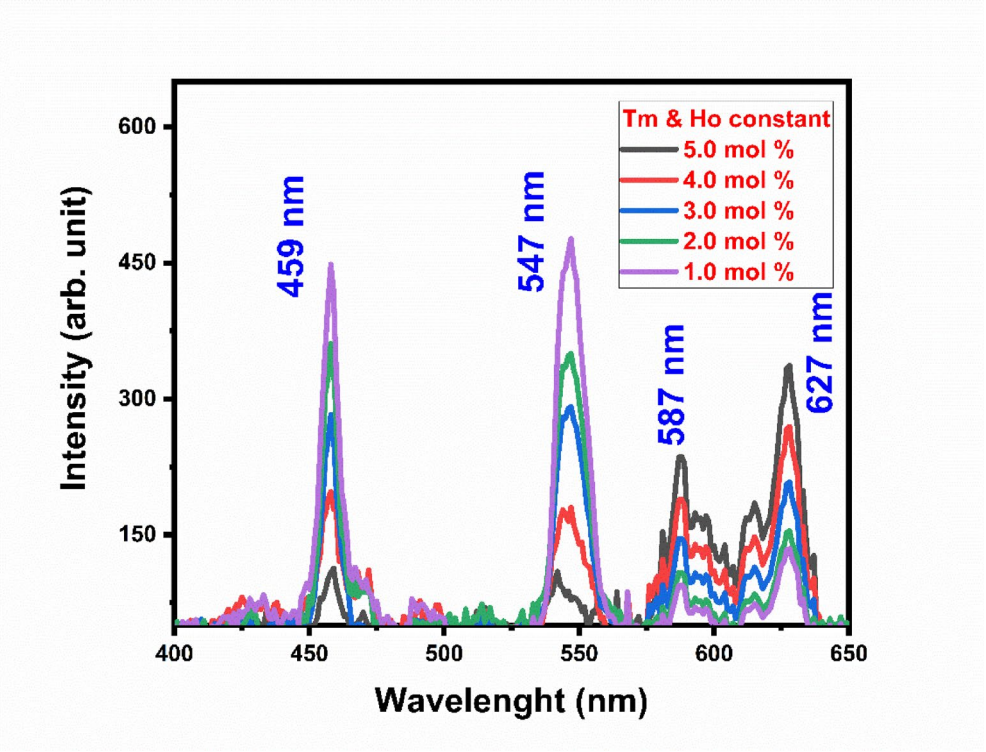

Fig. 30. Emission spectra of La_2O_3:Tm/Ho/Eu at excitation wavelength 363 nm.

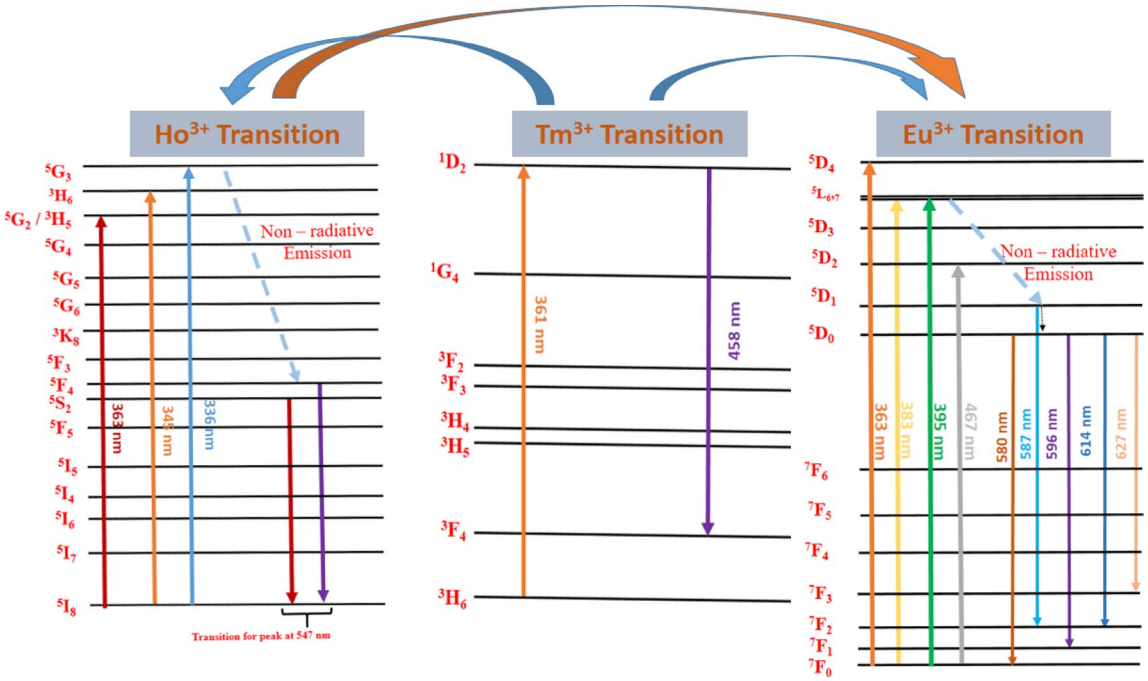

Fig. 31. Energy level diagram of Tm^{3+}, Ho^{3+}, Eu^{3+} triple doped La_2O_3 phosphor.

sr	Name	I_{Er}	I_{Ero}	Efficiency (%)
1	La_2O_3: Tm^{3+}(1.5 mol%)/Ho^{3+}(1.0 mol%)/Eu^{3+}(1.0 mol%)	237.6543	133.4	43.86804
2	La_2O_3: Tm^{3+}(1.5 mol%)/Ho^{3+}(1.0 mol%)/Eu^{3+}(2.0 mol%)	671.6266	152.7964	77.2498
3	La_2O_3: Tm^{3+}(1.5 mol%)/Ho^{3+}(1.0 mol%)/Eu^{3+}(3.0 mol%)	735.1859	206.1564	71.95861
4	La_2O_3: Tm^{3+}(1.5 mol%)/Ho^{3+}(1.0 mol%)/Eu^{3+}(4.0 mol%)	1353.832	266.8	80.29298
5	La_2O_3: Tm^{3+}(1.5 mol%)/Ho^{3+}(1.0 mol%)/Eu^{3+}(5.0 mol%)	842.2185	333.5	60.4022

Table 8. Energy transfer efficiency in La_2O_3:Tm/Ho/Eu.

La_2O_3:Tm

Figure 34 shows the CIE co-ordinate of La_2O_3:Tm. In CIE diagram the coordinates are in blue region that confirms the emission in green region. Table 11 shows the CIE co-ordinate, color purity and CCT of prepared sample. La_2O_3:Tm^{3+} phosphor have intense blue emission in blue region with high colour purity (>95%). La_2O_3:Tm^{3+} has narrow emission with single emission peak which makes it more suitable for laser application. La_2O_3:Tm^{3+}(0.5 mol%) and La_2O_3:Tm^{3+}(1.0 mol%) has commendable colour purity among all and low CCT values which makes it more beneficial to be used in decorative lighting, display technologies, and anti-counterfeiting coatings. Increasing concentration from 1.5 mol% to 2.5 mol% , colour purity decreases by small value which again makes it preferable prospect it useful in decorative lighting, display technologies, and anti-counterfeiting coatings.

La_2O_3:Tm/Ho

Figure 35 shows the CIE diagram of La_2O_3:Tm/Ho at excitation wavelength of 306 nm. As the concentration of Ho^{3+} ion increases from 0.5 mol% to 2.5 mol%, CIE coordinate start shifting from blue region to green region because of increasing green component in emission spectra as compared to blue components. CIE coordinate, CCT and color purity of La_2O_3:Tm/Ho at excitation wavelength 306 nm shown in Table 12. La_2O_3: Tm^{3+}(1.5 mol%)/Ho^{3+}(0.5 mol%) phosphor has emission in bluish green with comparably high purity around 60% - 65% which is suitable for anti-counterfeiting inks and display coatings. At La_2O_3: Tm^{3+}(1.5 mol%)/Ho^{3+}(1.5 mol%) phosphor is move toward the green region with moderate purity (~55.7%) with balanced blue and green emission. La_2O_3: Tm^{3+}(1.5 mol%)/Ho^{3+}(2.0 mol%) and La_2O_3: Tm^{3+}(1.5 mol%)/Ho^{3+}(2.5 mol%) phosphor has CIE coordinate move toward green region with decreasing the colour purity around (34% -38%) due to concentration effects, which can be leveraged for broad-spectrum. Overall, the concentration Ho^{3+} provide 0.5–1.5 mol% provides the best trade-off between vivid color and purity, while ≥2.0 mol% favours greener, less saturated emission.

Figure 36 show the CIE coordinate of La_2O_3:Tm/Ho at excitation wavelength 363 nm. As the concentration of Ho^{3+}, CIE coordinates start shifting from intense blue to intense green region. Table 13 consists of the detailed value of CCT, color purity, and CCT values for prepared sample. At La_2O_3: Tm^{3+}(1.5 mol%)/Ho^{3+}(0.5 mol%)

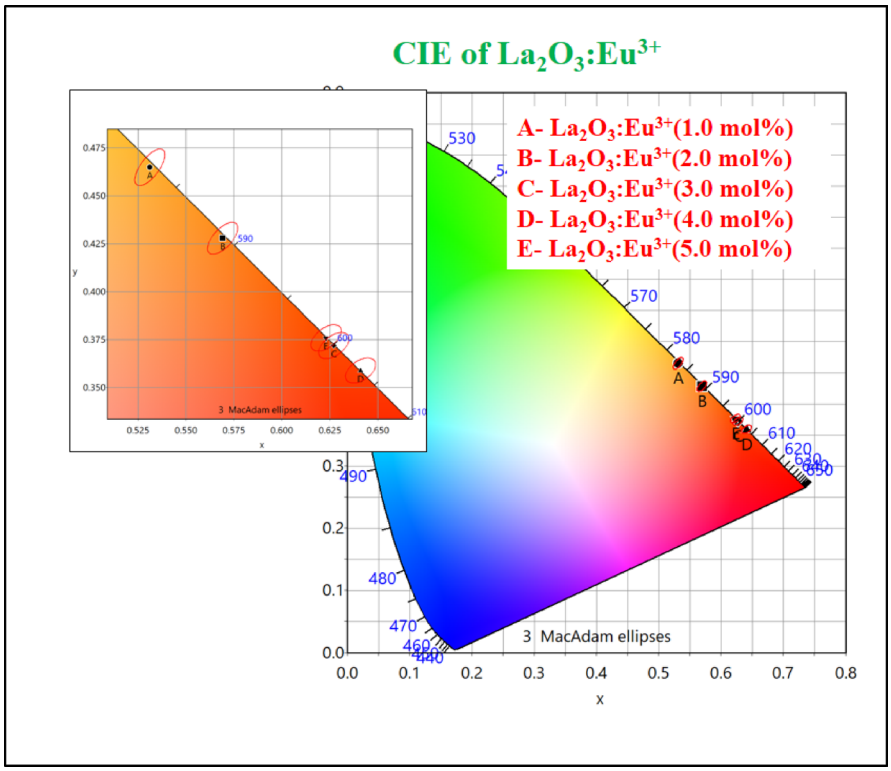

Fig. 32. CIE Diagram of La_2O_3:Eu.

$La_2O_3:Eu^{3+}$							
Sr. No	**Name**	**x**	**y**	**x_d**	**y_d**	**CCT (k)**	**Color Purity (%)**
1	$La_2O_3:Eu^{3+}$(1.0 mol%)	0.531	0.465	0.701	0.299	1155	68.08
2	$La_2O_3:Eu^{3+}$(2.0 mol%)	0.569	0.428	0.702	0.298	1728.58	71.89
3	$La_2O_3:Eu^{3+}$(3.0 mol%)	0.627	0.372	0.704	0.296	2267.34	81.59
4	$La_2O_3:Eu^{3+}$(4.0 mol%)	0.641	0.359	0.704	0.296	2530.67	84.60
5	$La_2O_3:Eu^{3+}$(5.0 mol%)	0.623	0.376	0.704	0.296	2229.14	80.77

Table 9. CIE coordinate, color purity, and CCT of La_2O_3:Eu.

phosphor has bluish emission as the emission is mainly due to Tm^{3+} emission with moderate colour purity of 34%. At La_2O_3: Tm^{3+}(1.5 mol%)/Ho^{3+}(1.0 mol%) has bluish- green emission with 31 % colour purity for cool display application. At La_2O_3: Tm^{3+}(1.5 mol%)/Ho^{3+}(1.5 mol%) and La_2O_3: Tm^{3+}(1.5 mol%)/Ho^{3+}(2.0 mol%) has emission in green-yellow with slightly improved purity (~32–36%), indicating balanced emission effective for tuneable lighting. Among all prepared phosphor La_2O_3: Tm^{3+}(1.5 mol%)/Ho^{3+}(2.5 mol%) has maximum colour purity around 48%, that makes it more prominent application in displays, bio-imaging.

La_2O_3:Tm/Ho phosphor is showing different emission color at different concentration of Ho^{3+} ion in host lattice. At low concentration one color is dominate while at high concentration different transitions activate due to cross relaxation and energy transfer, so color of emission is change. This property of multi color emission from single material can be useful in barcode application. In normal light barcode looks like normal black and white image but under 361 nm excitation different colour comes out according to Ho^{3+} concentration region. This dual mode appearance gives extra verification to barcode system. Normal barcode can be easily copy by printing but this type of multi emission barcode cannot be reproduce without exact knowledge of phosphor synthesis and doping level. That makes it highly secured system. Multi emission verification system is very useful in anti-counterfeiting. Prototype figure 37 shows barcode under room light and same barcode under 361 nm UV light, where different concentration region gives different color. By arranging phosphor with different concentration in barcode pattern we can prepare unique code which is very difficult to copy. Such type of feature is also useful in anti-counterfeiting of currency notes. Currency note looks normal in daylight but under UV source secret emission pattern will appear with multiple colors. This give two step verification for authentication. Such technology can also use in document, brand protection and other valuable goods. Advantage is one host material itself giving multiple emission colors only by changing Ho^{3+} concentration. This make system more

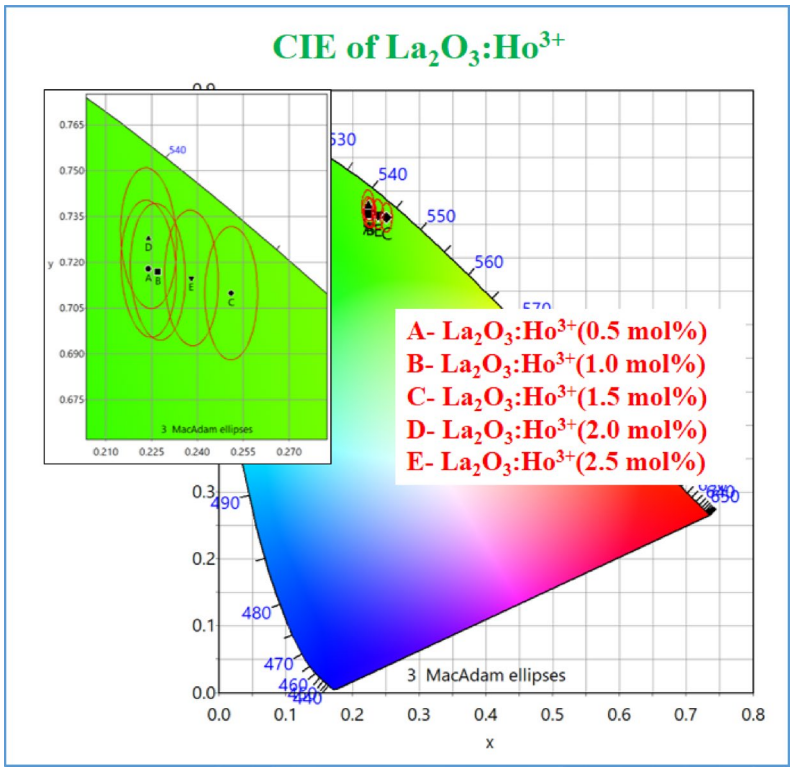

Fig. 33. CIE Diagram of La_2O_3:Ho.

La_2O_3:Ho^{3+}							
Sr. No	**Name**	**x**	**y**	**x_d**	**y_d**	**CCT (k)**	**Colour Purity (%)**
1	La_2O_3:Ho^{3+}(0.5 mol%)	0.224	0.718	0.273	0.718	7305.11	96.84
2	La_2O_3:Ho^{3+}(1.0 mol%)	0.227	0.717	0.280	0.712	7360.44	97.12
3	La_2O_3:Ho^{3+}(1.5 mol%)	0.251	0.710	0.287	0.705	6762.32	98.24
4	La_2O_3:Ho^{3+}(2.0 mol%)	0.224	0.728	0.280	0.712	7034.52	98.98
5	La_2O_3:Ho^{3+}(2.5 mol%)	0.238	0.715	0.280	0.712	7005.78	96.10

Table 10. CIE co-ordinate , Colour purity, and CCT of La_2O_3:Ho.

simple but strong against duplicate. Therefore La_2O_3:Tm/Ho phosphor with Ho^{3+} concentration dependent emission is a very promising material for barcode security, anti-counterfeit and advanced authentication system.

La_2O_3:Tm/Eu

Figure 38 shows the CIE diagram of La_2O_3:Tm/Eu. As the concentration of Eu ion increases, CIE coordinates start shifting from blue region to white region in CIE diagram. CIE coordinate, color purity, and CCT values are shown in table 14. La_2O_3:Tm^{3+}(1.5 mol%)/Eu^{3+}(1.0 mol%) and La_2O_3:Tm^{3+}(1.5 mol%)/Eu^{3+}(2.0 mol%) phosphor have moderate colour purity (~38–43%) with low CCT (~1900–2100 K), these values makes them useful for low intensity optoelectronic devices. With increasing concentration of Eu to 3 mol% and 4 mol%. Color purity slightly increases so it can be beneficial for manufacturing of warm white LEDs. La_2O_3: Tm^{3+}(1.5 mol%)/Eu^{3+}(5.0 mol%) has low colour purity among all prepared sample because of the incongruity between the red and blue colour. This is also useful in low-cost lighting and security ink application where low purity is needed.

La_2O_3:Ho/Eu

CIE co-ordinate of La_2O_3: Ho/Eu is shown in the figure 39. As the concentration of Eu^{3+} ion increases from 1.0 mol% to 5 mol%, CIE coordinate starts shifting from green region to red region. Color coordinates, color purity and CCT are shown in table 15. La_2O_3: Ho^{3+}(1.5 mol%)/Eu^{3+}(1.0 mol%) and La_2O_3: Ho^{3+}(1.5 mol%)/Eu^{3+}(2.0 mol%) phosphor coordinate starts shifting from green to red with relatively high CCT (~4700–5100 K), this makes this phosphor very suitable for WLEDs phosphor and display where mixed color output is needed. At La_2O_3: Ho^{3+}(1.5 mol%)/Eu^{3+}(3.0 mol%) and La_2O_3: Ho^{3+}(1.5 mol%)/Eu^{3+}(4.0 mol%) has shifting toward stronger red and lower CCT (~2900–4300 K)that makes it useful for warm white LEDs application. At La_2O_3:

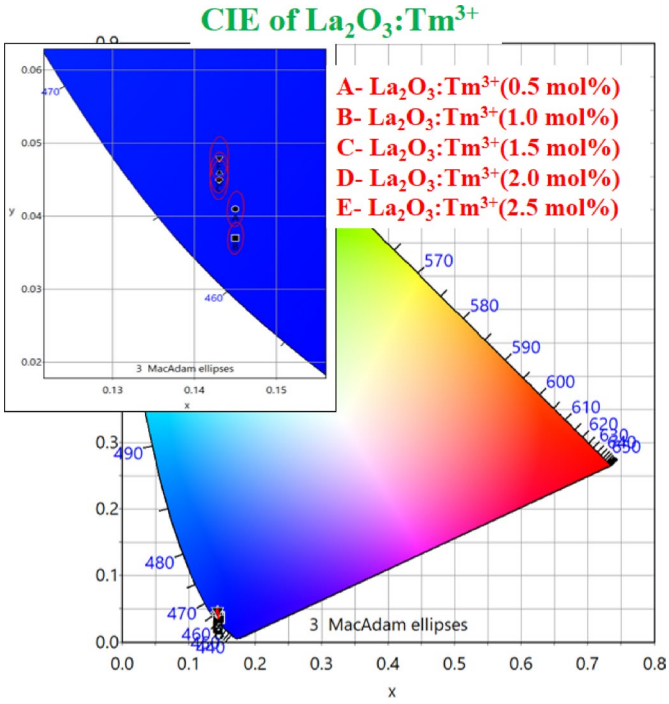

Fig. 34. CIE diagram of La_2O_3:Tm.

$La_2O_3:Tm^{3+}$							
Sr. No	**Name**	**x**	**y**	**x_d**	**y_d**	**CCT (k)**	**Colour Purity (%)**
1	$La_2O_3:Tm^{3+}$(0.5 mol%)	0.145	0.041	0.148	0.025	2813.01	96.29
2	$La_2O_3:Tm^{3+}$(1.0 mol%)	0.145	0.037	0.145	0.028	1767.06	97.66
3	$La_2O_3:Tm^{3+}$(1.5 mol%)	0.143	0.045	0.147	0.027	4589.36	95.94
4	$La_2O_3:Tm^{3+}$(2.0 mol%)	0.143	0.046	0.147	0.027	NA	95.68
5	$La_2O_3:Tm^{3+}$(2.5 mol%)	0.143	0.048	0.147	0.027	NA	95.17

Table 11. CIE coordinate, color purity, and CCT of La_2O_3:Tm.

Ho^{3+}(1.5 mol%)/Eu^{3+}(5.0 mol%), CIE coordinate approaches near (x=0.497, y=0.499) with the lowest CCT (~2504 K), which is ideal for solid-state lighting.

La_2O_3:Tm/Ho/Eu

Figure 40 is showing CIE diagram of La_2O_3:Tm/Ho/Eu. CIE co-ordinate of La_2O_3:Tm/Ho/Eu is in white or near white region. Color coordinate, color purity and CCT are shown in table 16. As concentration of Eu^{3+} ion increases, CIE coordinates start shifting from blue to white region in CIE diagram. At La_2O_3: Tm^{3+}(1.5 mol%)/Ho^{3+}(1.0 mol%)/Eu^{3+}(1.0 mol%) and La_2O_3: Tm^{3+}(1.5 mol%)/Ho^{3+}(1.0 mol%)/Eu^{3+}(2.0 mol%) lie in bluish green region where Tm and Ho ion dominance. This phosphor has low colour purity (8-11 %) with high CCT ~6400–7700 K) which makes this phosphor suitable for cool-white display applications. At La_2O_3: Tm^{3+}(1.5 mol%)/Ho^{3+}(1.0 mol%)/Eu^{3+}(3.0 mol%) and La_2O_3: Tm^{3+}(1.5 mol%)/Ho^{3+}(1.0 mol%)/Eu^{3+}(4.0 mol%) has co-ordinate in white region with the red component. CCT of prepared phosphor is decreases (~3700–4700 K), and color purity improves (~17–19%), indicating potential for tuneable white-light sources and decorative lighting. This phosphor has proportionated blue, green and red component in emission, which is favourable for white-light generation. At La_2O_3: Tm^{3+}(1.5 mol%)/Ho^{3+}(1.0 mol%)/Eu^{3+}(5.0 mol%) have emission shifting toward the reddish region with the lowest CCT (~2497 K). Importantly, this higher Eu^{3+} doping compensates for the red deficiency often observed in conventional WLEDs, thereby enabling the production of warm white light with improved color rendering. The La_2O_3: Tm^{3+}(1.5 mol%)/Ho^{3+}(1.0 mol%)/Eu^{3+}(3.0 mol%) composition is most suitable for WLEDs. Its CCT (~4759 K) and balanced CIE coordinates provide warm-white emission with moderate color purity, ideal for natural white light.

FTIR analysis

Figure 41 shows the FT-IR spectra of La_2O_3. Spectrum of La_2O_3 is recorded from 400 cm^{-1} to 4000 cm^{-1}. Spectra contain one major peak at 630 cm^{-1} is due to La–O vibration present in the La_2O_3. Some minor peaks are observed at 1367 cm^{-1} and 1485 cm^{-1} is due to –C=O vibration. Relatively small peak is observed at 3607 cm^{-1}

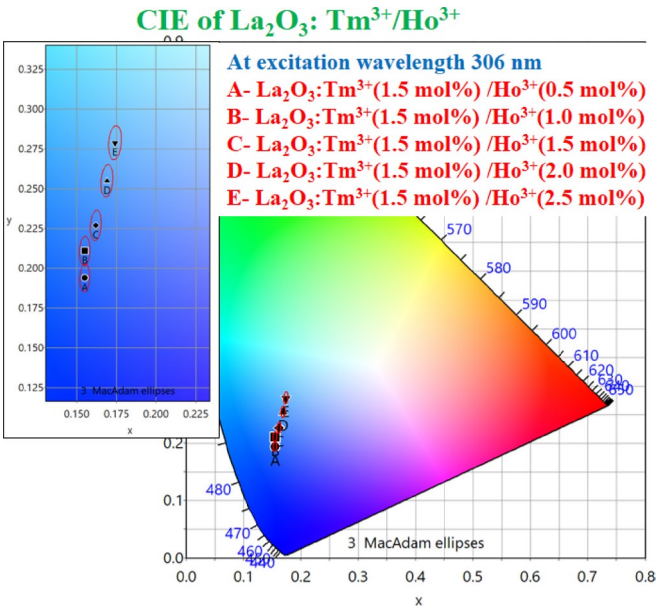

Fig. 35. CIE diagram of La_2O_3:Tm/Ho at excitation wavelength 306 nm.

La_2O_3: Tm^{3+}/Ho^{3+} at 306 nm							
Sr. No	**Name**	**x**	**y**	**x_d**	**y_d**	**CCT (k)**	**Colour Purity (%)**
1	La_2O_3: Tm^{3+}(1.5 mol%)/Ho^{3+}(0.5 mol%)	0.155	0.194	0.106	0.094	13,705,515.21	65.44
2	La_2O_3: Tm^{3+}(1.5 mol%)/Ho^{3+}(1.0 mol%)	0.155	0.211	0.119	0.068	13,705,515.21	59.82
3	La_2O_3: Tm^{3+}(1.5 mol%)/Ho^{3+}(1.5 mol%)	0.162	0.227	0.116	0.074	134,129.67	55.69
4	La_2O_3: Tm^{3+}(1.5 mol%)/Ho^{3+}(2.0 mol%)	0.169	0.255	0.280	0.712	47,359.82	38.73
5	La_2O_3: Tm^{3+}(1.5 mol%)/Ho^{3+}(2.5 mol%)	0.174	0.279	0.273	0.718	29,707.47	34.95

Table 12. CIE coordinate, color purity, and CCT of La_2O_3:Tm/Ho at 306 nm.

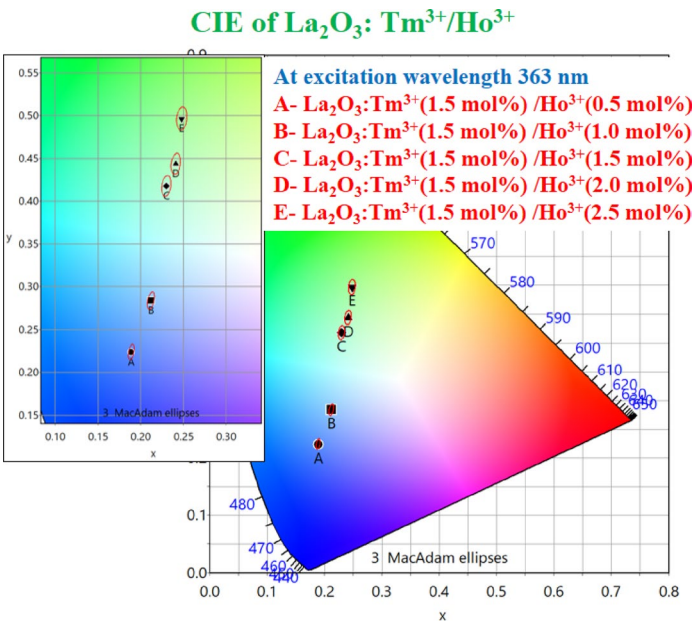

Fig. 36. CIE diagram of La_2O_3:Tm/Ho at excitation wavelength 363 nm.

La_2O_3: Tm^{3+}/Ho^{3+} at 363 nm							
Sr. No	Name	x	y	x_d	y_d	CCT (k)	Colour Purity (%)
1	La_2O_3: Tm^{3+}(1.5 mol%)/Ho^{3+}(0.5 mol%)	0.189	0.224	0.145	0.028	104,763.98	34.26
2	La_2O_3: Tm^{3+}(1.5 mol%)/Ho^{3+}(1.0 mol%)	0.212	0.284	0.145	0.028	33,888.44	31.08
3	La_2O_3: Tm^{3+}(1.5 mol%)/Ho^{3+}(1.5 mol%)	0.230	0.418	0.273	0.718	9275.05	32.10
4	La_2O_3: Tm^{3+}(1.5 mol%)/Ho^{3+}(2.0 mol%)	0.241	0.444	0.273	0.718	8184.02	36.01
5	La_2O_3: Tm^{3+}(1.5 mol%)/Ho^{3+}(2.5 mol%)	0.248	0.497	0.280	0.712	7525.85	48.16

Table 13. CIE coordinate, color purity, and CCT of La_2O_3:Tm/Ho at 363 nm.

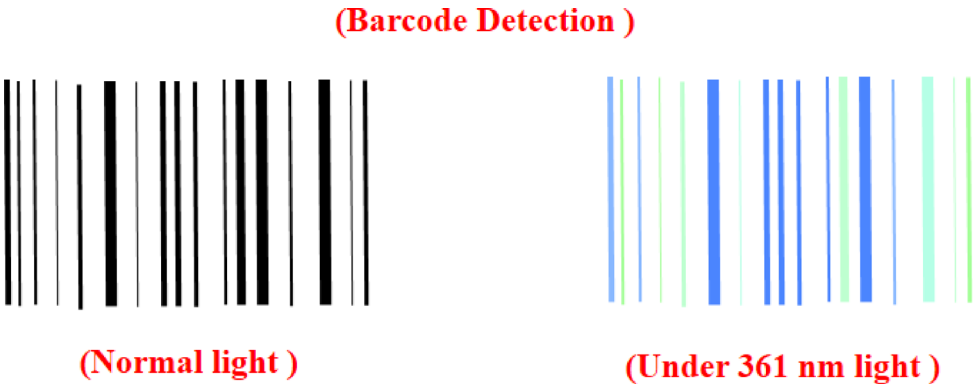

Fig. 37. La_2O_3:Tm/Ho phosphor applied barcode.

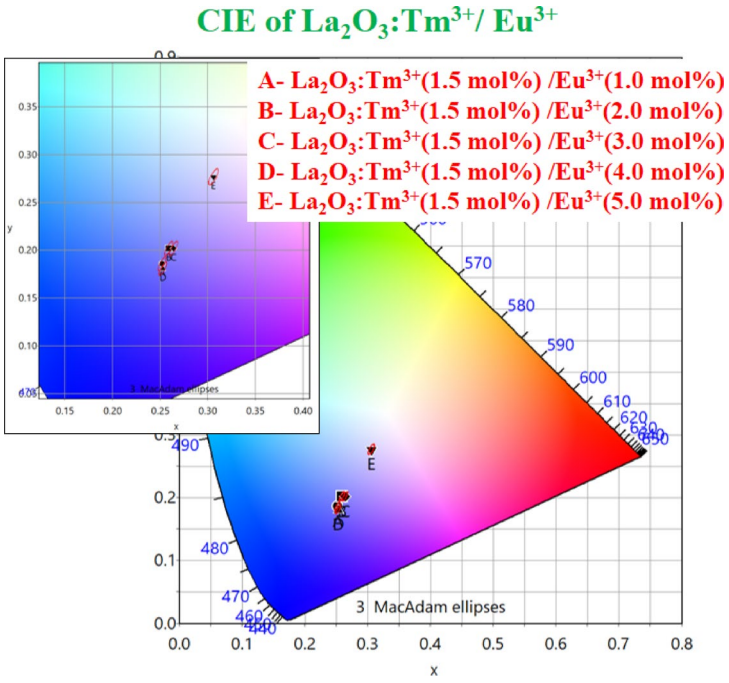

Fig. 38. CIE Diagram of La_2O_3:Tm/Eu.

is due to –O–H vibration in lattice. Tendency of absorbing the moisture from air ant turns into $La(OH)_3$ is small [50–52].

Conclusion

Photoluminescence property of La_2O_3 is single-doped with Tm, Ho and Eu, double-doped and triple-doped phosphor was studied. The phosphor was prepared by combustion synthesis method using hydrazine as fuel.

La_2O_3:Tm^{3+}/Eu^{3+}							
Sr. No	Name	x	y	x_d	y_d	CCT (k)	Color Purity (%)
1	La_2O_3:Tm^{3+}(1.5 mol%)/Eu^{3+}(1.0 mol%)	0.252	0.186	0.148	0.025	2143.21	42.77
2	La_2O_3: Tm^{3+}(1.5 mol%)/Eu^{3+}(2.0 mol%)	0.259	0.202	0.147	0.027	1937.9	37.67
3	La_2O_3: Tm^{3+}(1.5 mol%)/Eu^{3+}(3.0 mol%)	0.264	0.202	0.145	0.028	2041.07	37.07
4	La_2O_3: Tm^{3+}(1.5 mol%)/Eu^{3+}(4.0 mol%)	0.253	0.181	0.147	0.027	1750.49	44.19
5	La_2O_3: Tm^{3+}(1.5 mol%)/Eu^{3+}(5.0 mol%)	0.306	0.277	0.148	0.025	1758.54	11.81

Table 14. CIE coordinate, color purity, and CCT of La_2O_3:Tm/Eu.

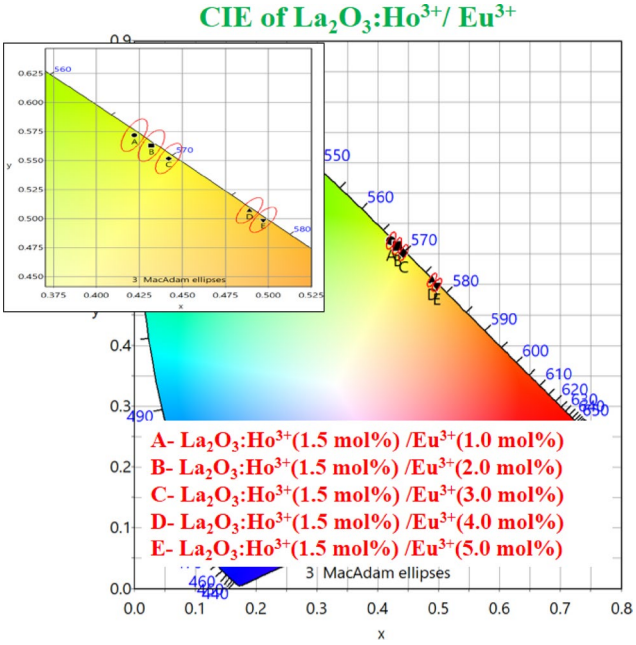

Fig. 39. CIE of La_2O_3: Ho/Eu.

La_2O_3: Ho^{3+}/Eu^{3+}							
Sr. No	Name	x	y	x_d	y_d	CCT (k)	Color Purity (%)
1	La_2O_3: Ho^{3+}(1.5 mol%)/Eu^{3+}(1.0 mol%)	0.422	0.572	0.273	0.718	5093.73	69.20
2	La_2O_3: Ho^{3+}(1.5 mol%)/Eu^{3+}(2.0 mol%)	0.432	0.563	0.273	0.718	4723.46	68.22
3	La_2O_3: Ho^{3+}(1.5 mol%)/Eu^{3+}(3.0 mol%)	0.442	0.552	0.266	0.724	4313.94	65.88
4	La_2O_3: Ho^{3+}(1.5 mol%)/Eu^{3+}(4.0 mol%)	0.489	0.507	0.704	0.296	2918.75	66.32
5	La_2O_3: Ho^{3+}(1.5 mol%)/Eu^{3+}(5.0 mol%)	0.497	0.499	0.704	0.296	2504.35	66.29

Table 15. CIE coordinate, color purity, and CCT of La_2O_3: Ho/Eu.

The pure and doped La_2O_3 phosphor shows hexagonal phase with space group -P6c2c. With doping of rare earth ions, XRD peaks are shifted towards larger angle side which indicates lattice contraction. Rietveld refinement result confirms that the lattice parameter decreases after doping and also change in z–coordinate of atom is observed. SEM image shows particles are agglomerated with irregular sizes and shapes with the average particle size around 12 µm. FTIR spectrum confirms the presence of La–O bonding in prepared phosphor. Tm, Ho and Eu ion doping gives blue, green and orange-red emissions respectively under UV excitation. Single crystallographic site of host helps Tm^{3+} ion to emit sharp peak in blue region. In La_2O_3:Ho^{3+} phosphor, energy gap between $^5F_4$ and $^5S_2$ level of Ho^{3+} (~ 200 cm^{-1}) is smaller than the phonon energy gap of La_2O_3 host (~ 400 cm^{-1}), so both levels to merge and give single emission band with increasing in FWHM. The energy transfer between Tm → Ho, Ho → Eu and Tm → Eu is studied in co-doped and tri-doped phosphor. The energy transfer efficiency of co-doped and triple doped phosphor is maximum at La_2O_3: Tm^{3+}(1.5 mol%)/Ho^{3+}(0.5 mol%), La_2O_3: Ho^{3+}(1.5 mol%)/Eu^{3+}(2.0 mol%), La_2O_3:Tm^{3+}(1.5 mol%)/Eu^{3+}(1.0 mol%), and La_2O_3: Tm^{3+}(1.5 mol%)/Ho^{3+}(1.0 mol%)/Eu^{3+}(4.0 mol%) about 54.52, 93.75, 90.70, and 77.24%respectivelyIn La_2O_3:Tm/Ho/Eu phosphors, efficient energy

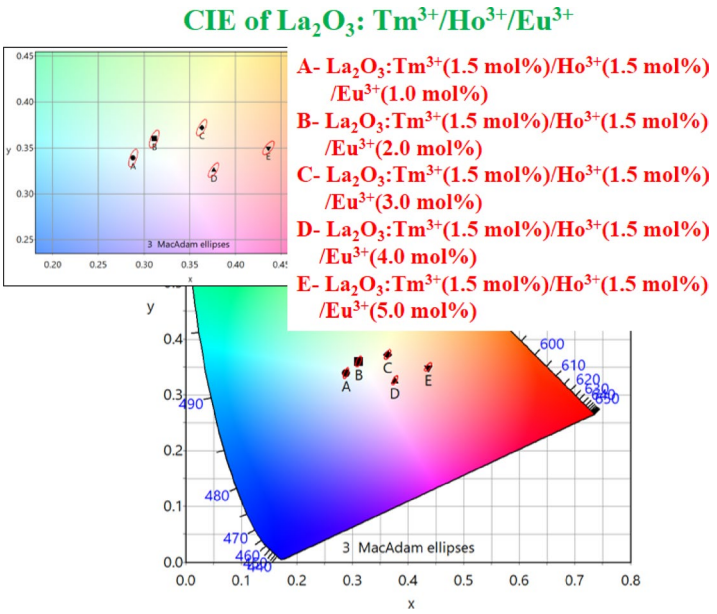

Fig. 40. CIE Diagram of La_2O_3:Tm/Ho/Eu.

La_2O_3: $Tm^{3+}/Ho^{3+}/Eu^{3+}$							
Sr. No	**Name**	**x**	**y**	**x_d**	**y_d**	**CCT (k)**	**Color Purity (%)**
1	La_2O_3: Tm^{3+}(1.5 mol%)/Ho^{3+}(1.0 mol%)/Eu^{3+}(1.0 mol%)	0.288	0.339	0.280	0.712	7778.77	8.00
2	La_2O_3: Tm^{3+}(1.5 mol%)/Ho^{3+}(1.0 mol%)/Eu^{3+}(2.0 mol%)	0.311	0.360	0.280	0.712	6377.15	11.05
3	La_2O_3: Tm^{3+}(1.5 mol%)/Ho^{3+}(1.0 mol%)/Eu^{3+}(3.0 mol%)	0.363	0.372	0.280	0.712	4759.22	19.38
4	La_2O_3: Tm^{3+}(1.5 mol%)/Ho^{3+}(1.0 mol%)/Eu^{3+}(4.0 mol%)	0.376	0.326	0.704	0.296	3715.36	16.90
5	La_2O_3: Tm^{3+}(1.5 mol%)/Ho^{3+}(1.0 mol%)/Eu^{3+}(5.0 mol%)	0.436	0.350	0.705	0.295	2497.06	32.97

Table 16. CIE coordinate, color purity, and CCT of La_2O_3:Tm/Ho/Eu.

absorption and energy transfer are observed. For white LEDs, the La_2O_3:Tm^{3+}(1.5 mol%)/Ho^{3+}(1.0 mol%)/Eu^{3+}(3.0 mol%) composition is preferable, with Tm^{3+} contributing blue, Ho^{3+} green, and Eu^{3+} red emission. For blue LEDs, La_2O_3:Tm is suitable; for green LEDs, La_2O_3:Ho; for red LEDs, La_2O_3:Eu; and La_2O_3:Tm/Ho is ideal for barcode applications due to its blue–green emission. Prepared phosphor can be applied in WLEDs, barcode security, and multicolor LED application.

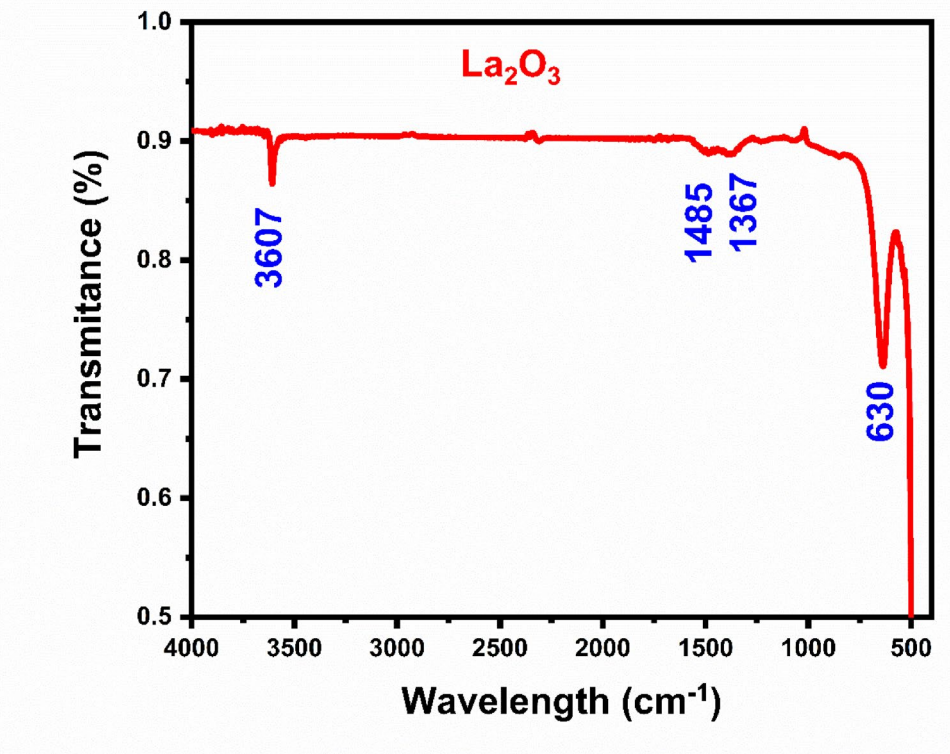

Fig. 41. FT-IR spectra of La_2O_3.

Data availability

The datasets generated and/or analysed during the current study are not publicly available due to intellectual property protection but are available from the corresponding author on reasonable request.

Received: 15 September 2025; Accepted: 12 November 2025
Published online: 08 December 2025

References

1. Shang, Y. et al. A novel red-emitting Cd2CaTeO6: Eu3+ phosphor with abnormal thermal quenching properties for personal identification and w-LEDs. *Spectrochim Acta Part A Mol Biomol Spectrosc* **338**, 126116. https://doi.org/10.1016/j.saa.2025.126116 (2025).
2. Hegde, M. et al. Investigations of Eu3+ activated calcium dialuminate based phosphor-in-glass as an inorganic color converter for solid-state lighting applications. *J Alloys Compd* **1037**, 182373. https://doi.org/10.1016/j.jallcom.2025.182373 (2025).
3. Lei, Y. et al. The application of w-LEDs and latent fingerprint visualization with a newly developed reddish-orange YNb2VO9:Eu3+ phosphor. *J Lumin* **283**, 121274. https://doi.org/10.1016/j.jlumin.2025.121274 (2025).
4. Jaiswal, V. V., Haranath. D. Phosphor Based Novel Invisible Ink for Knocking Out Fake Security Papers and Combat Counterfeiting. 1–24
5. Wang, Y. et al. Organic ionic host-guest phosphor with dual-confined nonradiation for constructing ultrahigh-temperature x-ray scintillator. *J Am Chem Soc* **147**, 11098–11107. https://doi.org/10.1021/jacs.4c16935 (2025).
6. Ma, R., Huang, W., Gong, X. & Deng, C. Tunable emission and photochromic properties of BaSrY4O8: Bi3+/Eu3+ phosphors for information encryption and anti-counterfeiting application. *Ceram Int* **51**, 13980–13991. https://doi.org/10.1016/j.ceramint.2025.01.234 (2025).
7. Kuang, Y. et al. Narrow-band green/red-emitting glass composites enabling highly stable patterned wheel for laser phosphor display. *Sci China Mater* **68**, 1822–1829. https://doi.org/10.1007/s40843-025-3361-1 (2025).
8. Tikale, R. V., Kadam, A. R., Michalska-Domańska, M. & Dhoble, S. J. Triple-doped Dy3+/Tb3+/Eu3+ activated Na2Ca4(PO4)3F halo-phosphors for next-generation WLEDs and solar cell efficiency enhancement. *Sci Rep* **15**, 27748. https://doi.org/10.1038/s41598-025-12538-x (2025).
9. Reddy, S. S., Nagabhushana, K. R., Tatumi, S. H. & Thejavathi, N. R. Investigating the optical and thermoluminescence properties of γ-irradiated Al2O3:Tb3+ phosphors for dosimetric applications. *J Lumin* **280**, 121067. https://doi.org/10.1016/j.jlumin.2025.121067 (2025).
10. Sidorov, N. V. et al. Concentration dependence of optical properties of double-doped LiTaO3:Cr3+:Nd3+ Crystals. *Materials (Basel)* https://doi.org/10.3390/ma18143218 (2025).
11. Jana, Y. et al. Tuning structural, spectroscopic and electronic properties of Mn4+ doped Y2GaSbO7 phosphor for optoelectronics and phototherapy applications. *J Alloys Compd* **1037**, 182169. https://doi.org/10.1016/j.jallcom.2025.182169 (2025).
12. Verma, A. et al. Tuning of luminescent properties of Zn1-xMgAl10O17:Eux nano phosphor. *J Alloys Compd* **764**, 1021–1032. https://doi.org/10.1016/j.jallcom.2018.06.023 (2018).
13. Verma, A. & Verma, A. Synthesis, characterization, mechano-luminescence, thermoluminescence, and antibacterial properties of SrMgAl10O17:Eu phosphor. *J Alloys Compd* **802**, 394–408. https://doi.org/10.1016/j.jallcom.2019.06.209 (2019).

14. Gangwar, B. P., Irusta, S. & Sharma, S. Effect of Bi3+ Ion concentration on physicochemical, optical and catalytic properties of one-pot combustion synthesized nanocrystalline bi-doped La2O3. *ChemistrySelect* **5**, 7548–7559. https://doi.org/10.1002/slct.201904435 (2020).
15. Moune, O. K., Jayasankar, C. K., Faucher, M. D. & Lejus, A. M. Analysis of the optical spectrum of Pr^{3+} in La_2O_3 and Pr_2O_3. *Mater Sci Forum* **315–317**, 415–423. https://doi.org/10.4028/www.scientific.net/msf.315-317.415 (1999).
16. Zhang, X. S. et al. Facile fabrication and spectroscopic study of the energy transfer effect of Pr 3 + and Tm 3 + codoped La 2O 3 nanorod arrays. *Mater Lett* **76**, 165–168. https://doi.org/10.1016/j.matlet.2012.02.079 (2012).
17. Shah, K., Murthy, K. V. R. & Chakrabarty, B. S. Investigation of UV emission and energy transfer process in Ce3+, Gd3+, Pr3+ and their combination doped nano crystallite La2O3 phosphors. *Results Opt* **11**, 100413. https://doi.org/10.1016/j.rio.2023.100413 (2023).
18. Minami, T. et al. PL and EL Characteristics in New Blue Emitting La2O3:Bi Phosphor Thin Films. *ECS Trans* **16**, 39–45. https://doi.org/10.1149/1.3106670 (2009).
19. Fukada, H. et al. Blue PL and EL emissions from Bi-activated binary oxide thin-film phosphors. *Thin Solid Films* **518**, 3067–3070. https://doi.org/10.1016/j.tsf.2009.08.014 (2010).
20. De Mello, D. C. et al. The vibronic spectroscopy and luminescence concentration quenching of the Pr3+ ion in La2O3, LaOF and LiYF4. *J Phys Chem Solids* **56**, 267–276. https://doi.org/10.1016/0022-3697(94)00175-8 (1995).
21. Shi, Z., Yang, Q., Lu, S. & Zhang, H. Spectral properties of Pr3+:La2O3 ceramics. *Adv Mater Res* **299–300**, 633–636. https://doi.org/10.4028/www.scientific.net/AMR.299-300.633 (2011).
22. Xu, Z. et al. Preparation and luminescence of La2O3:Ln3+ (Ln3+ = Eu3+, Tb3+, Dy3+, Sm 3+, Er3+, Ho3+, Tm3+, Yb 3+/Er3+, Yb3+/Ho3+) microspheres. *RSC Adv* **3**, 1410–1419. https://doi.org/10.1039/c2ra22480a (2013).
23. Etafo, N. O. et al. Influence and applications of refractive index on the catalytic perfomance of photo-responsive materials. *Environ Surfaces Interfaces* **3**, 237–264. https://doi.org/10.1016/j.esi.2025.09.004 (2025).
24. Tikale, R. V., Koparkar, A. D., Kadam, A. R. & Dhoble, S. J. *J Fluoresc* https://doi.org/10.1007/s10895-024-04127-4 (2025).
25. Tikale, R. V., Kadam, A. R., Halwar, D. K. & Dhoble, S. J. Luminescence investigation of red emitting CaAlSiO4F: Eu3+ doped phosphor for white LEDs based on oxyfluoride matrix. *Mater Lett X* **21**, 100224. https://doi.org/10.1016/j.mlblux.2023.100224 (2024).
26. Khode, P. P., Parauha, Y. R., Nikolay, N. G. & Dhoble, S. J. Enhancement in photoluminescence properties of La2O3:Bi3+ phosphor by codoping with Na+, Cs+. *J Mol Struct* **1346**, 143116. https://doi.org/10.1016/j.molstruc.2025.143116 (2025).
27. Etafo, N. O. et al. Blue-Emitting SrLaAlO4: Ce phosphors obtained by combustion synthesis. *Mater Sci Forum* **1112**, 131–137. https://doi.org/10.4028/p-5A41Hx (2024).
28. Chen, C. X. et al. Investigation of the rigid structure, luminescence properties of stable CaY2Al4SiO12: Bi/Tb/Sm phosphors toward wLEDs application. *Ceram Int* **51**, 28839–28847. https://doi.org/10.1016/j.ceramint.2025.04.093 (2025).
29. Nair, G. B., Swart, H. C. & Krishnan, R. Activation of Tm3+ single-photon NIR-to-NIR upconversion luminescence through Yb3+ doping in Tm2WO6 phosphor. *Opt Mater (Amst)* **158**, 116459. https://doi.org/10.1016/j.optmat.2024.116459 (2025).
30. Verma, A. et al. Yttrium aluminum garnet based novel and advanced phosphor synthesized by combustion route activated by Dy, Eu, and Tb rare earth metals. *J Mater Sci Mater Electron* **34**, 1–24. https://doi.org/10.1007/s10854-023-10022-8 (2023).
31. Verma, A., Verma, A., Bramhe, G. V. & Sahu, I. P. Optical studies of the Ba1-XMgAl10O17:Eux phosphors synthesis by combustion route. *J Alloys Compd* **769**, 831–842. https://doi.org/10.1016/j.jallcom.2018.07.371 (2018).
32. Verma, A. et al. Achieving structural, photoluminescence, temperature dependent photoluminescence and thermo-luminescence properties of SrAl2O4:Dy3+Eu3+ phosphor for WLED application. *Emergent Mater* **7**, 3029–3051. https://doi.org/10.1007/s42247-024-00773-3 (2024).
33. Feng, J., Gao, Y. & Ren, H. Red-shift of the photoluminescent emission and enhancement of the internal quantum efficiency by co-doping Gd3+ in Tb3Al5O12: Ce3+ phosphors for warm WLEDs. *J Solid State Chem* **341**, 125042. https://doi.org/10.1016/j.jssc.2024.125042 (2025).
34. Mahfuzul Haque, M. et al. Modulation of optoelectronic properties of WO3 thin film via Cr doping through RF co-sputtering. *Inorg Chem Commun* **177**, 114300. https://doi.org/10.1016/j.inoche.2025.114300 (2025).
35. Tikale, R. V., Kadam, A. R., Mathur, A. & Dhoble, S. J. Combustion assisted optical and structural investigation of Dy3+/Eu3+ co-doped KMg3Si3AlO10F2 phosphor by energy transfer mechanism. *Inorg Chem Commun* https://doi.org/10.1016/j.inoche.2024.112146 (2024).
36. Parauha, Y. R., Yadav, R. S. & Dhoble, S. J. Enhanced photoluminescence via doping of phosphate, sulphate and vanadate ions in Eu3+ doped La2(MoO4)3 downconversion phosphors for white LEDs. *Opt Laser Technol* **124**, 105974. https://doi.org/10.1016/j.optlastec.2019.105974 (2020).
37. Parauha, Y. R. & Dhoble, S. J. Color-tunable luminescence, energy transfer behavior and I-V characteristics of Dy3+, Eu3+ co-doped La(PO4) phosphors for WLEDs and solar applications. *New J Chem* **46**, 6230–6243. https://doi.org/10.1039/d2nj00232a (2022).
38. Khan S, Parauha YR, Halwar DK, Dhoble SJ (2021) Rare Earth (RE) doped color tunable phosphors for white light emitting diodes. In: Journal of Physics: Conference Series. IOP Publishing Ltd
39. Tikale, R. V., Kadam, A. R., Mathur, A. & Dhoble, S. J. Sm3+ activated Ba3LaNa(PO4)3F fluorophosphate phosphor: Synthesis, characterization and their photoluminescence investigation for warm WLEDs. *Chem Phys Impact* **9**, 100741. https://doi.org/10.1016/j.chphi.2024.100741 (2024).
40. Tikale, R. V., Kadam, A. R. & Dhoble, S. J. Optical properties and crystal structure analysis of Sr3AlO4F:Sm3+, Eu3+ phosphors: an approach towards color tunability. *J Mater Sci Mater Electron* **34**, 1868. https://doi.org/10.1007/s10854-023-11356-z (2023).
41. Saeed, N. A. M., Swart, H. C. & Coetsee, E. Photoluminescence up-conversion and temperature sensing of YOF and V-YOF single-doped Ho3+. *J Lumin* **287**, 121453. https://doi.org/10.1016/j.jlumin.2025.121453 (2025).
42. Kumar, A. et al. Infrared and UV assisted visible up/down-conversion in Gd2O3:Ho3+/Yb3+micro-rods for highly efficient photovoltaic performance of dye-sensitized solar cell. *J Mol Struct* **1341**, 142559. https://doi.org/10.1016/j.molstruc.2025.142559 (2025).
43. Tripathi, R., Modanwal, S., Mishra, H. & Fanai, A. L. Optical characterization and color-tuneable up-conversion emissions in Ho3+/Yb3+ Co-doped zinc tellurite glasses. *Ceram Int* **51**, 35857–35864. https://doi.org/10.1016/j.ceramint.2025.05.307 (2025).
44. Deshmukh, H. S. & Muley, G. G. Enhanced upconversion emission in Nd, Yb, Er and Ho tetra-doped Y2O3 phosphor. *Results Opt* **15**, 100656. https://doi.org/10.1016/j.rio.2024.100656 (2024).
45. Yuan, B., Li, M. & Zhang, C. Calcination-assisted hydrothermal crystallization and comparative up-/down-conversion luminescence of RE3+ (RE=Ho, Er and Tm)-doped YbNbO4 and Yb3NbO7. *Mater Today Commun* **41**, 110860. https://doi.org/10.1016/j.mtcomm.2024.110860 (2024).
46. Wang, X. et al. Crystal structural effects on up/down-conversion luminescence properties of GdInO3:Tm,Yb perovskite phosphors for effective dual-mode anti-counterfeit applications. *Opt Express* **32**, 14018–14032. https://doi.org/10.1364/OE.518016 (2024).
47. Chen, Y. et al. Boosting the Downconversion Luminescence of Tm3+-Doped Nanoparticles for S-Band Polymer Waveguide Amplifier. *Nano Lett* **24**, 1399–1405. https://doi.org/10.1021/acs.nanolett.3c04725 (2024).
48. Etafo, N. O. Advancements of Lanthanide-doped Phosphors in Solid-state Lighting Applications. *Curr Phys* https://doi.org/10.2174/0127723348280880240115054806 (2024).
49. Khode, P. P., Kadam, A. R., Nikolay, N. G. & Dhoble, S. J. Structural investigation and color tunability in Dy3+, Sm3+co-doped La2O3 phosphors for WLED applications. *J Mol Struct* https://doi.org/10.1016/j.molstruc.2025.143030 (2025).

50. Tsoutsou, D. et al. Infrared spectroscopy and X-ray diffraction studies on the crystallographic evolution of La2O3 films upon annealing. *Microelectron Eng* **85**, 2411–2413. https://doi.org/10.1016/j.mee.2008.09.033 (2008).
51. Subramanian, P. & David, S. A. Biosynthesis of La2O3 Nanoparticles using Lawsonia inermis Leaf Extract. *Uttar Pradesh J Zool* **45**, 161–169. https://doi.org/10.56557/upjoz/2024/v45i184434 (2024).
52. Alfryyan, N. et al. Sodium fluoroborate glass loaded with fixed CoO and variable La2O3: Fabrication, Physical, FTIR, and dielectric characteristics. *J Electron Mater* **54**, 1467–1474. https://doi.org/10.1007/s11664-024-11478-y (2025).

Acknowledgements
Part of co-authors (SJD and PPK) are thankful to Department Science and Technology (DST), India for the finical support.

Author contributions
Praful P. Khode: Methodology, Investigation, Writing—original draft. Aditi Deshmukh: Methodology. Mateusz Czerwiński: Methodology, Analysis. Marta Michalska-Domańska: Analysis, Writing—review & editing. S. J. Dhoble: Supervision, Writing—review & editing.

Additional information
Correspondence and requests for materials should be addressed to M.M.-D. or S.J.D.

Reprints and permissions information is available at www.nature.com/reprints.

Publisher's note Springer Nature remains neutral with regard to jurisdictional claims in published maps and institutional affiliations.